

A phloem-localized *Arabidopsis* metacaspase (AtMC3) improves drought tolerance

Eugenia Pitsili^{1,2} , Ricardo Rodriguez-Trevino³, Nerea Ruiz-Solani¹, Fatih Demir^{4,5}, Elizabeth Kastanaki³, Charlene Dambire⁶, Roger de Pedro-Jové¹ , Dominique Vercammen², Jose Salguero-Linares¹ , Hardy Hall⁷, Melissa Mantz^{4,5} , Martin Schuler³, Hannele Tuominen⁷ , Frank Van Breusegem² , Marc Valls^{1,8} , Sergi Munné-Bosch^{9,10} , Michael J. Holdsworth⁶ , Pitter F. Huesgen^{4,5} , Antia Rodriguez-Villalon³  and Nuria S. Coll^{1,11} 

¹Centre for Research in Agricultural Genomics (CRAG), CSIC-IRTA-UAB-UB, Campus UAB, Bellaterra, 08193 Barcelona, Spain; ²Department of Plant Systems Biology, Department of Plant Biotechnology and Bioinformatics, Flanders Institute for Biotechnology, Ghent University, 9052 Ghent, Belgium; ³Group of Plant Vascular Development, Swiss Federal Institute of Technology (ETH) Zurich, 8092 Zurich, Switzerland; ⁴Central Institute for Engineering, Electronics and Analytics, ZEA-3, Forschungszentrum Jülich GmbH, 52425 Jülich, Germany; ⁵Cologne Excellence Cluster Cellular Stress Response in Aging-Associated Diseases (CECAD), Department of Chemistry, University of Cologne, Medical Faculty and University Hospital, Institute of Biochemistry, Joseph-Stelzmann-Str. 26, 50931 Cologne, Germany; ⁶School of Biosciences, University of Nottingham, Loughborough LE12 5RD, UK; ⁷Department of Plant Physiology, Umeå Plant Science Centre, Umeå University, 901 87 Umeå, Sweden; ⁸Department of Genetics, Universitat de Barcelona, 08028 Barcelona, Spain; ⁹Department of Evolutionary Biology, Ecology and Environmental Sciences, Faculty of Biology, Universitat de Barcelona, Avinguda Diagonal 643, 08028 Barcelona, Spain; ¹⁰Institute of Research in Biodiversity (IRBio-UB), Universitat de Barcelona, 08028 Barcelona, Spain; ¹¹Consejo Superior de Investigaciones Científicas (CSIC), 08001 Barcelona, Spain

Summary

Author for correspondence:

Nuria S. Coll

Email: nuria.sanchez-coll@cragenomica.es

Received: 4 November 2022

Accepted: 9 May 2023

New Phytologist (2023)

doi: 10.1111/nph.19022

Key words: abscisic acid, *Arabidopsis thaliana*, drought, hypoxia, metacaspases, osmotic stress, phloem.

- Increasing drought phenomena pose a serious threat to agricultural productivity. Although plants have multiple ways to respond to the complexity of drought stress, the underlying mechanisms of stress sensing and signaling remain unclear. The role of the vasculature, in particular the phloem, in facilitating inter-organ communication is critical and poorly understood.
- Combining genetic, proteomic and physiological approaches, we investigated the role of AtMC3, a phloem-specific member of the metacaspase family, in osmotic stress responses in *Arabidopsis thaliana*. Analyses of the proteome in plants with altered AtMC3 levels revealed differential abundance of proteins related to osmotic stress pointing into a role of the protein in water-stress-related responses.
- Overexpression of AtMC3 conferred drought tolerance by enhancing the differentiation of specific vascular tissues and maintaining higher levels of vascular-mediated transportation, while plants lacking the protein showed an impaired response to drought and inability to respond effectively to the hormone abscisic acid.
- Overall, our data highlight the importance of AtMC3 and vascular plasticity in fine-tuning early drought responses at the whole plant level without affecting growth or yield.

Introduction

Plants, as sessile organisms, have evolved ways to endure water scarcity and periods of drought stress. However, the tissue-specific mechanisms underlying the adaptation of plant growth and architecture to limited water conditions are not completely understood. Only by improving our understanding of the contribution of each tissue in plant acclimation to such a complex stress as drought, we will be able to translate this knowledge into biotechnological and breeding solutions and improve crop performance in the field (Tenorio Berrío *et al.*, 2022).

When facing drought stress, plants arrest growth, close stomata, and begin accumulating osmoprotectant molecules to prevent excessive water loss and minimize cellular damage (Gupta

et al., 2020). As a result of stomatal closure, photosynthesis is arrested, leading to a negative carbon balance and carbon deprivation which may cause mortality in the long run (Thalmann & Santelia, 2017). Many of these physiological responses are triggered by the synthesis and perception of the hormone abscisic acid (ABA), an essential orchestrator of abiotic stress resistance mechanisms that regulate water status to protect cell systems and induces the expression of a gene network that includes dehydration-tolerant proteins (Kuromori *et al.*, 2018, 2022).

To coordinate an efficient response to water deprivation at the organismal level, plants rely on their vascular system connecting distantly separated organs. In higher plants, such as *Arabidopsis thaliana* (hereafter *Arabidopsis*), the vascular system comprises xylem and phloem tissues. While the main function of xylem is

root-to-shoot transport of water and nutrients, the phloem distributes photoassimilates and growth regulators throughout the entire plant body. It is well accepted that drought stress triggers the translocation of root-synthesized ABA to the shoot through the xylem, while coordinating stomatal closure (Hartung *et al.*, 2002; Takahashi *et al.*, 2020). Recent studies have demonstrated that drought stress promotes endodermal production of ABA (Ondzighi-Assoume *et al.*, 2016; Ramachandran *et al.*, 2018; Bloch *et al.*, 2019), which is then translocated to the xylem where it modulates the signaling cascades governing its specification and differentiation (Ramachandran *et al.*, 2021). Most of these studies have focused on the modification of xylem architecture as a response to the stress, whereas in the case of phloem, knowledge is limited to the fact that drought-associated osmotic imbalance may promote the release of water from phloem cells and eventually collapse tissue transport. While loss of xylem conductivity is a hallmark of plant death, it has been proposed that the timing of phloem collapse could determine the revival capacity of the plants after drought, making this tissue an important factor for forecasting the plant behavior under water scarcity (Sevanto, 2018).

In Arabidopsis, two types of conductive elements constitute phloem tissue, protophloem, and metaphloem sieve elements (PSE and MSE, respectively), whose survival depends on the activity of neighboring companion cells (CCs; Fig. 1a,b). Unlike metaphloem, the molecular mechanism underpinning protophloem specification and differentiation has been extensively studied during the last decade (Rodríguez-Villalón, 2016; Seo *et al.*, 2020). PSEs are the first cells to differentiate within the root meristem and they orchestrate the development of their neighboring tissues. The functional association between CC and PSEs provides developmental plasticity to root cells safeguarding the functionality of the phloem tissues (Gujas *et al.*, 2020; Otero *et al.*, 2022). Early differentiation of PSEs is required for the root meristematic unloading of sugars and hormones (Band *et al.*, 2014). Since sugars constitute the energy source for root development, defects in protophloem differentiation are reflected in an impaired meristematic activity and, in turn, postembryonic root growth (Truernit *et al.*, 2012; Rodríguez-Villalón *et al.*, 2014). Less studied is the plasticity of the tissue in response to environmental stresses, although proteomic profiling of exudates from plants exposed to drought stress has revealed that the phloem transports water-deficit-related signals (Ogden *et al.*, 2020).

Metacaspases are a group of cysteine proteases that participate in various stress responses (Tsiatsiani *et al.*, 2011; Minina *et al.*, 2017). This protein family is found in plants and lower eukaryotes and have some structural resemblance to the animal cell death regulators known as caspases, although their mode of action is considerably different, as they are calcium-dependent and cleave substrates after a lysine or an arginine (Chang & Yang, 2000; Watanabe & Lam, 2005; McLuskey & Mottram, 2015). In plants, metacaspases can be divided into type I and type II based on the presence/absence of a prodomain, respectively. The role of metacaspases has been mostly investigated in the context of stress responses and regulated cell death in

Arabidopsis, which carries nine metacaspase genes, three type I (AtMC1/AtMCAIa-AtMC3/AtMCAIc) and six type II (AtMC4/AtMCAIIa-AtMC9/AtMCAIIIf; Vercammen *et al.*, 2004; He *et al.*, 2008; Coll *et al.*, 2010; Bollhöner *et al.*, 2013; Hander *et al.*, 2019).

Here, we show that the previously uncharacterized Arabidopsis type I metacaspase AtMC3/AtMCAIc displays specific expression in the phloem vascular tissue. Altered AtMC3 levels leads to differential accumulation of stress-related proteins, indicating that AtMC3 is specifically involved in regulating osmotic stress responses. We demonstrate that a phloem-localized metacaspase contributes to drought tolerance by affecting vascular tissue differentiation and maintaining effective long-distance transport under osmotic stress conditions. Additionally, we provide evidence that reduced AtMC3 levels affect plant sensitivity to ABA.

Materials and Methods

Plant material and growth conditions

Arabidopsis thaliana (L.) Heynh. accession Col-0 was used (genotypes shown in Supporting Information Table S1). Surface-sterilized seeds were sown in Murashige and Skoog (MS) media with vitamins and without sucrose. After 48 h of vernalization, plates were grown vertically under long day (LD) conditions (16 h : 8 h, light : dark; 22°C, 60% relative humidity) unless specified otherwise. DNA C-TAB extraction protocol (Murray & Thompson, 1980) was used for all plant genotyping experiments (primers for genotyping shown in Table S2).

DNA constructs

For reporter line *proAtMC3:GUS-GFP*, Gateway cloning was used. Briefly, a 1500-bp promoter region of *AtMC3* was cloned into the binary vector pBGWFS7. *proUBQ10:AtMC3-GFP*, *proAtMC3:AtMC3-GFP*, *proUBQ10:AtMC3-C230A-GFP*, and *proAtMC3:AtMC3-C230A-GFP* constructs were generated using the GREENGATE cloning strategy as described previously (Lampropoulos *et al.*, 2013). To generate the catalytic inactive version of the gene, the Quick Site Mutagenesis Kit (Agilent Technology, Santa Clara, CA, USA). Plants were transformed using *Agrobacterium tumefaciens* (GV3101)-mediated floral dip as described previously (Zhang *et al.*, 2006). Homozygous transgenic lines were selected either on MS media supplemented with 20 µg ml⁻¹ Basta (glufosinate-ammonium) or by red/green. Primers used for cloning are shown in Table S2.

CRISPR mutagenesis

The target sequence was selected using CRISPOR (Haeussler *et al.*, 2016). DNA backbone fragments of a total length of 500 bp contained: 20 bp of the target sequence neighboring the PAM sequence, *attB* sequences, *tracrRNA*, U6 promoter, and restriction sites (gBlocks[®], IDT). The *gBlock* sequence was introduced to *pDONR207* using BP clonase II enzyme (Thermo, Waltham, MA, USA). Three gRNAs were combined in one vector after

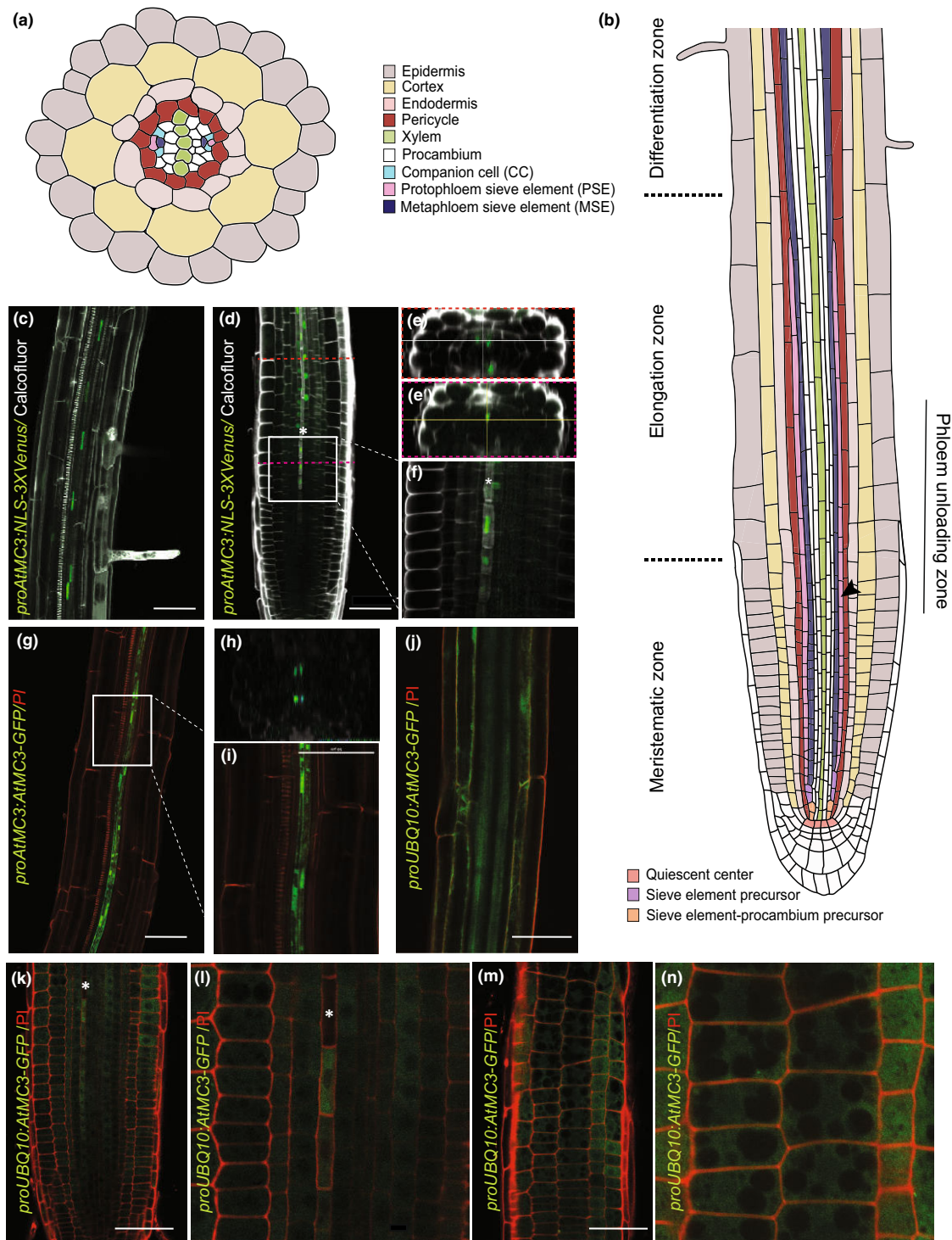


Fig. 1 *AtMC3* shows phloem-specific expression. Schematic representation of (a) a radial view and (b) longitudinal view of a primary root of *Arabidopsis thaliana* with color-coded cell types. (c–f) Expression pattern of *AtMC3* gene as revealed by *proAtMC3:NLS-3xVENUS* construct with confocal microscopy (c) in the root differentiation zone and (d–f) in the root meristem of 6-d-old seedlings. Nuclear-localized mVENUS signals (green) are co-visualized with calcofluor staining (white). (e, e') Radial observations of different zones of the root indicated by color in (d). (f) Magnification of the vascular tissue from the meristematic zone at the protophloem enucleation point. (g) Localization of arabidopsis metacaspase (*AtMC3*) protein monitored with *proAtMC3:AtMC3-GFP* in the root differentiation zone in 7-d-old seedlings. Translational fusions with GFP signals (green) are co-visualized with propidium iodide (red). (h) Radial observation of the root. (i) Magnification of (g) for the cytoplasmic companion cell (CC) visualization. (j–n) Localization of *AtMC3* monitored with *proUBQ10:AtMC3-GFP* in the root of 7-d-old seedlings. Translational fusions with GFP signals (green) are co-visualized with propidium iodide (PI; red). (j) Differentiation zone of the root. (k, l) Meristematic zone focusing on the vasculature with magnification. Asterisks indicate the first enucleated sieve element (SE). (m, n) Meristematic zone focusing on the epidermal cells with magnification. Bars, 50 μ m.

digestion with restriction enzymes BamHI/PstI/SalI. The *pDONR207* vector containing the triple gRNAs sequences and the single gRNA sequence was then transferred into the *pDe-CAS9-DsRED* vector (Morineau *et al.*, 2017) via LR reaction (Thermo). *A. tumefaciens* (GV3101)-mediated floral dip was used to deliver the construct to WT plants as described previously (Zhang *et al.*, 2006).

Confocal analysis

Confocal laser scanning microscopy was performed using a Leica SP2 AOBS inverted confocal microscope or a Zeiss LSM 780. For the detection of fluorescent signal eGFP, 488 nm excitation and 505–550 nm emission were used and for propidium iodide 561 nm excitation and 595–620 nm emission were used. Calcofluor-stained samples (Ursache *et al.*, 2018) were excited at 405 nm, and emission was collected at 425–475 nm. Different Z stacks and transverse optical versions were obtained using IMAGEJ software.

Cotyledons vein pattern

Cotyledons of 6-d-old seedlings were submerged for 1 h in a 3 : 1 95% ethanol: acetic acid solution. Subsequently, they were washed twice for 30 min with 70% ethanol and incubated overnight at 4°C with 100% ethanol. 10% NaOH was added for 1 h, and the samples were left at 37°C before Clear-See was added as a final step. Digital pictures were obtained on a Leica DM6 epi-fluorescence microscope.

β-Glucuronidase (GUS) staining

Seedlings were harvested from plates at the 2-cotyledon stage and then fixed/stained as described (Bollhöner *et al.*, 2013). Five seedlings were mounted in 50% glycerol and were viewed at 10×. Hypocotyls from mature plants were stained with GUS solution, fixed in 50% ethanol, 10% formaldehyde, 5% acetic acid, embedded in LRwhite + PEG, and sectioned at 18 μm with a microtome after embedding in Entellan.

Transcriptional analysis

Tissue was collected separately from roots and cotyledons of 7-d-old seedlings. RNA extraction, cDNA synthesis, and reverse transcription quantitative PCR (RT-qPCR) were performed as described previously using 2 μg of RNA template (Salguero-Linares *et al.*, 2022). *EIF4a* (AT4G18040) was used as reference gene, and calculations were done with the 2^{-C_t} method (Livak & Schmittgen, 2001). Primers are shown in Table S3.

Proteomic and terminomic analysis

For terminome analysis, c. 600 mg of 7-d-old roots was harvested per genotype. HUNTER N-terminome analysis was performed after stable isotope labeling by reductive demethylation as described (Weng *et al.*, 2019).

For identification of interactors, WT and plants overexpressing *AMC3* (*proUBQ10::AtMC3-GFP*) were grown for 3 wk before subjected to water withdrawal. Leaf tissue was collected from plants well-watered and subjected to drought for 5 d. Protein extraction buffer (20 mM Tris-HCl, pH 7.5, 150 mM NaCl, 1 mM EDTA, Glycerol, 1% Triton X-100, 0.1% SDS, and 5 mM DTT) supplemented with a 1 : 100 dilution of plant protease inhibitor cocktail (Roche) was added to the ground samples and centrifuged 20 min at 6000 g at 4°C. The supernatant was collected and centrifuged at 11 000 g, 4°C. The supernatant was again collected, and protein concentrations were measured using Bradford (Bio-Rad) and equalized at 1.5 μg. Fifty microliters of anti-GFP magnetic beads (Miltenyi Biotec, Bergisch Gladbach, Germany) were added to the protein extracts and incubated for 1 h at 4°C in a rotary mixer. Magnetic beads were immobilized on a magnetic separator (Miltenyi Biotec) and washed and eluted according to the manufacturer's instructions. Three independent plants were bulked in each of the four independent biological replicates.

LC/MS/MS and data analysis

LC-MS/MS analysis was performed with an UltiMate 3000 RSCL nano-HPLC system (Thermo) online coupled to an Impact II Q-TOF mass spectrometer (Bruker, Billerica, MA, USA) via a CaptiveSpray Ion Source boosted with an ACN-saturated nitrogen gas stream. For preHUNTER samples, peptides were loaded on an Acclaim PepMap100 C18 trap column (3 μm, 100 Å, 75 μm i.d. × 2 cm; Thermo) and separated on an Acclaim PepMap RSLC C18 column (2 μm, 100 Å, 75 μm i.d. × 50 cm; Thermo) with a 2 h elution protocol that included an 80 min separation gradient from 5% to 35% solvent B (solvent A: H₂O + 0.1% FA, solvent B: ACN + 0.1% FA) at a flow rate of 300 nl min⁻¹ at 60°C. For IP samples, peptides were loaded on a μPAC pillar array trap column (1 cm length; PharmaFluidics) and separated on a μPAC pillar array analytical column (50 cm flowpath; PharmaFluidics). Line-mode MS spectra were acquired in mass range 200–1400 *m/z* with a Top14 method.

For analysis of preHUNTER and IP data, peptides were identified by matching spectra against the UniProt *Arabidopsis thaliana* protein database (release 2020_2) with appended MAXQUANT contaminant entries using the Andromeda search engine integrated into the MAXQUANT software package (v.1.6.10.43) with standard settings (Tyanova *et al.*, 2016). Further analysis was performed using the PERSEUS software package (v.1.6.14.0 or v.1.6.15.0). For preHUNTER proteins changing, at least 50% in abundance (\log_2 fold change < -0.58 or > 0.58) supported by a *t*-test *P*-value < 0.05 were considered as differentially accumulating. For AtMC3 IP analysis, significant differences between the individual experimental groups followed by analysis for significant changes using the ANOVA test (*P*-value < 0.05) followed by Tukey's post hoc test (FDR < 0.05).

ABA sensitivity assays

Approximately 100 seedlings were sown on MS plates without or with ABA at concentrations of 1 or 2 μM. Germination was

quantified after 8 d as the number of seeds that showed both radical protrusion and elongation.

For senescence measurements, detached cauline leaves from 5-wk-old plants were soaked in distilled water without/with 50 μM ABA for 3 d. Each leaf was weighed and mechanically homogenized. Two milliliters of 80% acetone was added, and samples were incubated at 4°C for 16 h in the dark. Chlorophyll *a* was calculated as described previously (Lichtenthaler, 1987).

To measure stomatal aperture, cotyledons were collected from 10-d-old seedlings and immediately immersed in a stomata-opening buffer with 10 mM KCl, 0.2 mM CaCl_2 , and 10 mM Mes-KOH (pH 6.15) for 2^{1/2} h under continuous white light at 22°C. ABA was then added into the buffer to a final concentration of 10 μM and the cotyledons were collected after 30 min. Guard cells were photographed using a LEICA DM6 microscope, and stomatal widths were measured with IMAGEJ.

Drought stress for scoring plant survival

Seedlings grown in MS-agar plates were transferred after 7 d to individual to pots containing 30 \pm 0.5 g of substrate (plus 1 : 8 v/v vermiculite and 1 : 8 v/v perlite). For each biological replicate, 40 plants of every genotype were grown for 3 wk before subjected to severe drought stress. Water was withheld for 8 d followed by re-watering. After the 6-d recovery period, the surviving plants were counted and photographed. Every genotype was tested at least in five independent replicates.

Physiological parameters and chlorophyll fluorescence

Plants were grown for 3 wk on individual pots containing 30 \pm 0.5 g of substrate (plus 1 : 8 v/v vermiculite and 1 : 8 v/v perlite) before being subjected to water withholding. Relative water content (RWC, %) was calculated according to the formula: $(\text{FW}-\text{DW})/(\text{TW}-\text{DW})$. Water was withheld until reaching 30%, 60%, 75%, and 90% water loss. Pots were weighted daily to monitor evapotranspiration (CW). Water-saturated soil was weighted initially (SW), and several pots with soil were placed in the oven for 72 h to calculate the dry weight (DW). Field capacity was calculated for each pot daily as $(\text{CW}-\text{DW})/(\text{SW}-\text{DW})$.

Photosynthesis efficiency was measured in well-watered and drought-treated plants at 40% and 6% field capacity. After dark adaptation, the kinetics of chlorophyll fluorescence in whole rosettes were monitored by measuring F_0 in the dark and F_m with initial saturation pulse using Imaging PAM M-series, MAXI version device. F_v/F_m and F'_v/F'_m (PSII efficiency) ratio for the maximum quantum efficiency upon dark and light conditions was calculated according to the manufacturer's instructions (Walz, Effeltrich, Germany).

Osmotic stress assays

For salt treatments, seedlings were grown for 3 d before transferred to MS plates containing 0, 50, or 100 mM NaCl concentration for seven additional days. Primary root length was measured 10 d after germination using IMAGEJ. Emerged lateral roots were counted using an Olympus DP71 stereomicroscope.

For sorbitol treatments, seeds were sown on 1/2 Murashige & Skoog (MS) medium supplemented with 1% sucrose and grown for 3 d in continuous light conditions and then transferred to 1/2 MS plates without sucrose containing 120 mM sorbitol for three additional days before confocal microscopy analysis. Primary root length was measured at 6 d after germination using IMAGEJ software.

CFDA

A stock of 5-(and-6)-carboxyfluorescein diacetate (CFDA) was prepared by dissolving 5 mg ml^{-1} CFDA (Sigma Aldrich) in acetone. Plants were grown vertically for 3 d before being transferred into 120 mM sorbitol for three additional days before the treatment. A droplet of CFDA was supplied to the cotyledons of 6-d-old seedlings after pinching them with fine tweezers. Fluorescence intensity was imaged after 1 h of incubation using a Leica stereomicroscope with GFP filter and was calculated as mean intensity values from a circular region in the area above the meristematic zone of the root tip using Fiji/IMAGEJ.

Hypoxic stress assays

Seedlings were grown in 1/4 strength MS plates for 4 d under short day (conditions: $T=20^\circ\text{C}$, light intensity = 110 $\mu\text{mol m}^{-2} \text{s}^{-2}$). Plates without lids were then transferred to a desiccator (hypoxia chamber) in the dark, and nitrogen gas was introduced at a flow rate of 41 min^{-1} , for 4 h. Oxygen within the chamber was reduced to < 0.3% within 1 h. Treatment and survival rate was measured as previously (Hartman *et al.*, 2019).

Hormone quantification

Three-week-old plants were subjected to drought stress by water withholding for 5–6 d. Approximately 100 mg of leaf material were harvested from plants under drought and well-watered conditions and ground to a fine powder in liquid nitrogen. IAA, ABA, SA, JA, GA1, GA3, GA4, GA7, ACC, tZ, tZR, OPDA, IPA, and melatonin were quantified as described previously (Müller & Munné-Bosch, 2011).

Results

AtMC3 is a phloem-specific metacaspase

AtMC3 expression is specifically detected in vascular tissues of all plant organs in young seedlings, as revealed by transgenic Arabidopsis lines carrying the *AtMC3* promoter fused to GUS (*proAtMC3:GUS*; Fig. S1a–d) and as reported previously (Kwon & Hwang, 2013; Otero *et al.*, 2022). *AtMC3* expression was mostly restricted to the phloem, as shown by transverse cuts either in the stem or the hypocotyl (Fig. S1e–l). In the hypocotyl phloem, the expression appears to be strongest in a small cell type that represents CCs (Fig. S1g). To determine the cell-specific expression of *AtMC3*, Arabidopsis reporter lines containing nuclear-localized fluorescent VENUS protein under the

endogenous *AtMC3* promoter were generated (*proAtMC3:NLS-3xVENUS*). Confocal microscopy analysis of *proAtMC3:NLS-3xVENUS* roots confirmed the phloem pole-specific expression of *AtMC3* (Fig. 1c–f). Initiation of *proAtMC3*-driven *NLS-3xVENUS* expression within the root meristem was observed in PSE differentiating cells before their enucleation. After completion of the PSE differentiation process, *NLS-3xVENUS* was detected in the CCs of the elongation zone (Fig. 1d–f). Additionally, *proAtMC3*-driven *NLS-3xVENUS* expression was also specifically detected at the CCs from the differentiation zone onwards in the root (Fig. 1c).

To identify whether *AtMC3* expression corresponded to the site of *AtMC3* protein accumulation or transport through the vasculature, we generated transgenic lines stably expressing *proAtMC3:AtMC3-GFP*. Confocal analysis revealed that *AtMC3-GFP* specifically localizes in CCs in the differentiation zone and the signal could also be detected in the differentiating PSE in the meristematic zone (Figs 1g–i, S2a,b). As expected, *AtMC3* overexpression (*proUBQ10:AtMC3-GFP*) resulted in protein accumulation (Fig. 1j–n). Interestingly, GFP signal was not detected in enucleated SEs, suggesting that *AtMC3* cannot be transferred through the vasculature (Fig. 1l). Subcellularly, *proAtMC3*-driven *AtMC3* expression appeared evenly distributed throughout the cytoplasm (Fig. 1i,l,n) as indicated by the absence of the signal in the nucleus or the vacuoles. This is consistent with the localization of most of the metacaspases studied (Coll *et al.*, 2010; Bollhöner *et al.*, 2013; Hander *et al.*, 2019). Mutation of the predicted catalytic cysteine to an alanine in *AtMC3* (C230A; Fig. 2a) did not affect protein localization, (Fig. S2c–f), but resulted in increased accumulation of the protein (Fig. S2g), as observed previously for other metacaspases, such as *AtMC1* (Lema Asqui *et al.*, 2018).

Altered expression of *AtMC3* enhances seedling root growth without affecting phloem formation

To investigate the role of *AtMC3* within phloem tissues, CRISPR genome editing technology was employed to generate targeted mutations (Fauser *et al.*, 2014). Homozygous lines were obtained, each containing a different mutation in the *AtMC3* sequence that resulted in C-terminal truncations of the proteins due to frame alteration and generation of premature stop codons (Fig. 2a): *atmc3* #6.10 and #13.3. The latter presents a 763-bp deletion and was therefore selected for further functional analysis. *AtMC3* transcript levels demonstrated that only *atmc3*#13.3 plants are null mutants, incapable of producing full-length transcripts, while transgenic lines overexpressing *AtMC3* show enhanced levels of expression compared with wild-type (WT) plants (Fig. 2b).

To determine whether *AtMC3* is involved in plant growth or development, a detailed phenotypic characterization of *atmc3* mutants and overexpressor lines was performed. No significant differences were observed at the adult stage in terms of rosette size, plant height or inflorescence tissues (Figs 2c, S3a). However, at the seedling stage, both the null mutant and overexpressor lines exhibited a larger root meristem size compared with WT plants,

which translated into significantly longer roots (Fig. 2d,e; Ruiz Sola *et al.*, 2017). The smaller increase in root length observed for the second independent overexpressor line could be due to lower accumulation of *AtMC3* (Figs 2d, S2g). Furthermore, no differences were observed in lateral root formation or cotyledon vein pattern, which are typically associated with phloem defects, between the lines examined (Fig. S3c,d). Confocal microscopy analysis showed no defects in protophloem continuity (Fig. S3b), as evidenced by the continuous nuclear expression of *GFP* driven by the protophloem-specific promoter *COTYLEDON VASCULAR PATTERN 2* (*CVP2*; Fig. 2f,f'). Additionally, protophloem-mediated unloading in the root tip was not affected in the *atmc3*#13.3 mutant as demonstrated by the detection and quantification of *GFP* expressed under the companion cell-specific promoter *SUCROSE TRANSPORTER 2* (*SUC2*) in root meristem cells (Fig. 2g,g',h).

Since other metacaspases have also been shown to be expressed in the vasculature (Kwon & Hwang, 2013), one potential explanation for the lack of phenotype could be redundancy between *AtMC3* and other family members. Transcriptional analysis revealed that there was no compensatory expression of any other metacaspase family member in the *atmc3*#13.3 mutant background (Fig. S4a). Nonetheless, redundancy cannot be completely ruled out, since post-translational differences could occur in other metacaspases as a result of *AtMC3* mutation.

atmc3 Null mutant displays reduced sensitivity to the stress hormone abscisic acid (ABA)

To assess the effects of altered *AtMC3* levels on plants and whether its putative protease function is relevant, a proteomic approach was employed. The initial objective was to compare the degradomes of the *atmc3*#13.3 mutant and *AtMC3* overexpressor to WT plants, aiming to identify potential proteolytic substrates of *AtMC3*, as the protein is predicted to be a cysteine protease (Uren *et al.*, 2000). We performed High-efficiency Undecanal-based N Termini Enrichment (HUNTER; Weng *et al.*, 2019) using root tissue. However, the N-terminome enrichment experiment did not reveal any *bona fide* *AtMC3* substrates – that is, proteins cleaved after an arginine and/or lysine. Nonetheless, analysis of the digested proteome before enrichment provided protein abundance measurements in the different *AtMC3* backgrounds (Dataset S1). Pairwise comparisons between the different genotypes revealed a core set of proteins with their levels consistently altered (> 50% change in abundance, *t*-test *P*-value < 0.05) in the *AtMC3* overexpressing line when compared to both WT and *atmc3* mutant plants (Fig. 3a,b; Dataset S2, S3). Most of the significantly accumulating proteins in the overexpressing line were related to responses to stressful environmental conditions (Fig. 3c; Dataset S4). In particular, four positive regulators of the response to hypoxia and oxidative stress (ACX1, At4g19880, FAD-OXR, and DJ1A), one positive regulator of drought stress responses (BGLU18), and a positive regulator of defense responses (KTI4) were found in higher abundance (Fig. 3d). Consistently, three negative regulators of ABA signaling (BGLU22, BFRUCT4, and SASP), a negative regulator of

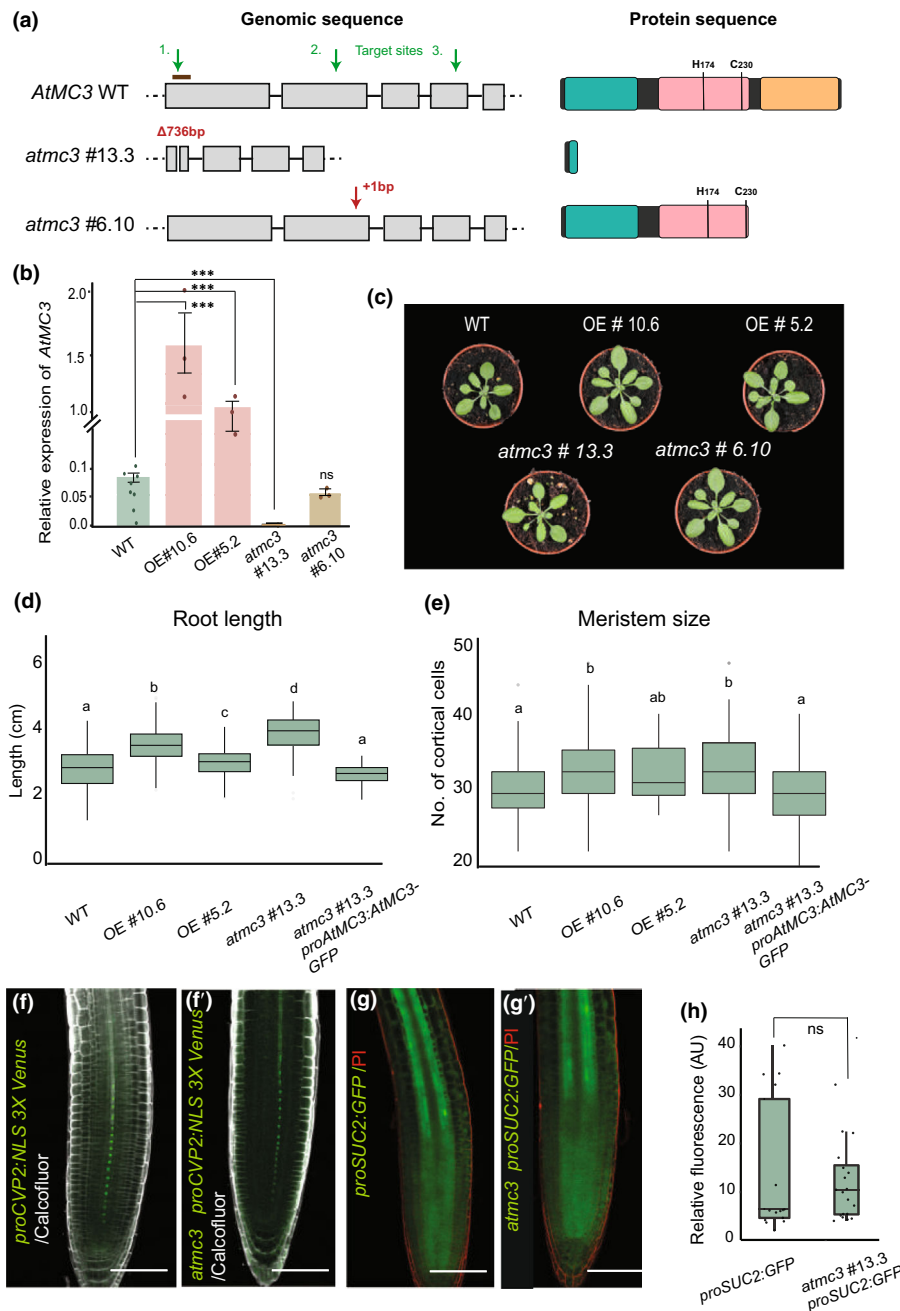


Fig. 2 Characterization of the *AtMC3* CRISPR mutant. (a) Schematic representation of the *AtMC3* gene and protein structure of Col-0 wild-type (WT) and CRISPR mutant plants generated. Target sites chosen are indicated with green arrows and mutations generated are indicated in red on top of the gene loci affected. Brown line indicates the fragment amplified for the detection of gene expression by quantitative PCR. The different gray boxes represent the exons of the gene sequence. In the protein structure, green color represents the metacaspase prodomain, pink and orange colors indicate the catalytic p20 and p10 domains, respectively. The predicted catalytic sites are indicated with H for Histidine in position 174 and C for Cysteine in position 230. (b) Expression analysis for the *AtMC3* gene in WT, overexpressor (independent lines #10.6, #5.2), *atmc3*#13.3, and *atmc3*#6.10 plants, in 7-d-old seedlings roots. Data are means (\pm SE) of three biological replicates. Significant differences from WT were determined by Student's *t*-test: ***, $P < 0.0005$. (c) Rosette phenotypes of 3-wk-old plants for WT, two independent overexpressor lines, and two CRISPR mutant lines. (d) Root length of 7-d-old seedlings and (e) meristematic size of 6-d-old seedlings measured from WT, overexpressors, *atmc3*#13.3 mutant, and complemented plants with the gene under the endogenous promoter (*atmc3*#13.3 *proAtMC3:AtMC3-GFP*). Different lowercase letters depict significant differences in a one-way ANOVA plus a Tukey's HSD test between the genotypes: $P < 0.05$. Box plots represent six biological replicates with $n \geq 40$ roots per genotype f, f') Representative pictures from root tips for observation of PSE nuclei in WT and *atmc3* #13.3 mutant plants carrying *proCVP2:NLS-3xVENUS*. Nuclear-localized VENUS signals (green) are co-visualized with calcofluor staining (white; g, g') Representative pictures from root tips of WT and *atmc3* #13.3 mutant plants carrying *proSUC2:GFP*. Nuclear-localized GFP signals (green) are co-visualized with PI staining (red). (h) Quantification of unloaded cytosolic GFP of plants from (g, g'), (\pm SE). Fluorescence intensity was quantified over a rectangular area 100 μ m above the QC; $n \geq 12$ roots per genotype. ns, non-significant.

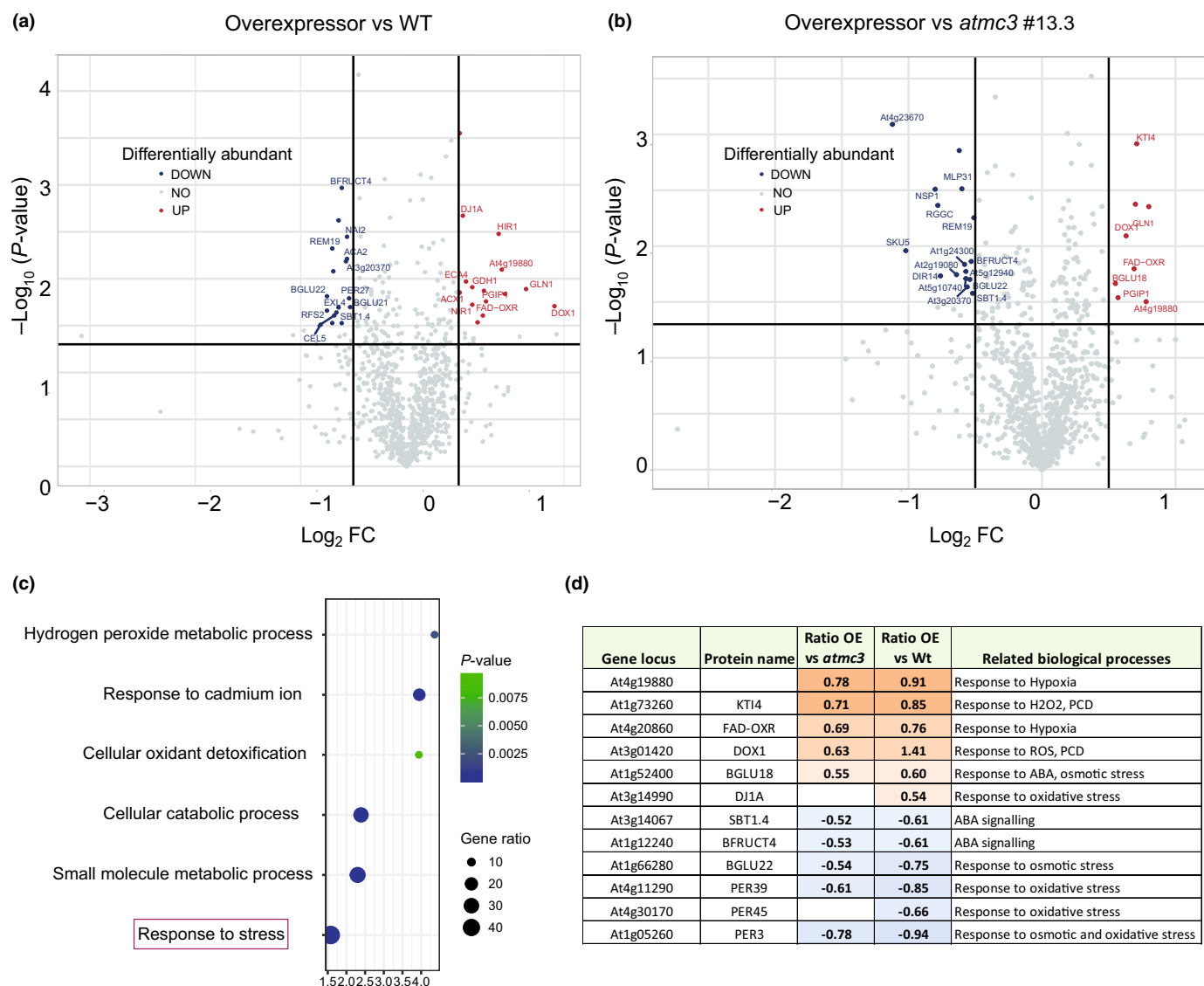


Fig. 3 Proteomic analysis in root tissue showed differential abundance of stress-related proteins depending on AtMC3 protein levels. Volcano plots of peptide abundance in (a) overexpressor line of *AtMC3* (OE #10.6) compared with WT plants and (b) overexpressor line of *AtMC3* (OE #10.6) compared with the *atmc3*#13.3 mutant plants. N-terminal peptides with significantly reduced or increased abundance (Student's *t*-test: *P*-value < 0.05; and \log_2 FC < -0.5 or > 0.5) are highlighted with blue and red color, respectively. Results are means from four independent biological replicates. For the complete list of proteins that were deregulated by the different expression levels of *AtMC3*, see Supporting Information Dataset S1–S3. (c) Gene ontologies (GO) terms representing enriched biological processes derived from proteins significantly deregulated in *AtMC3* overexpressing plants compared with WT samples (*t*-test, ANOVA analysis). The most general GO provided by PLAZA (Van Bel *et al.*, 2022) was plotted along with its corresponding gene number, fold enrichment, and *P*-value < 0.05. For the complete list of GO terms, see Dataset S4. (d) Summary of stress-related proteins which were found differentially abundant in the comparisons performed. Biological processes are presented according to the GO following: Response to oxidative stress: (GO:0006979), (GO:0042744), (GO:1900409) Response to osmotic stress: (GO:0009269), (GO:0071472), (GO:0009651), (GO:0009414), (GO:0030104), ABA signalling: (GO:0009687), (GO:0009738), (GO:0009789), (GO:0009737), PCD: (GO:0008219), (GO:0012501), ROS: (GO:0034614), (GO:0042542).

drought responses (NAI2), and several peroxidases responding to oxidative stress (PER3, PER29, and PER45) were identified among the proteins depleted in the *AtMC3* overexpressor line (Fig. 3d). The *atmc3* mutant was also compared with WT, but application of the selection criteria identified a single differentially accumulating protein; the chloroplastic serine peptidase CGEP, which was significantly more abundant in WT plants (Fig. S5; Dataset S5). The lack of striking differences between WT and mutant plants could be explained by the discrete expression of *AtMC3* in WT plants, concentrated in the phloem tissue,

which rendered impossible to detect native protein levels by immunoblot.

Proteomic data suggested that *AtMC3* may be involved in ABA signaling and drought/hypoxia responses, both of which have a dramatic impact in the osmotic balance of the plant (Munns, 2002; Tan & Zwiazek, 2019; Zahra *et al.*, 2021). To test this hypothesis, we first examined whether *atmc3*#13.3 mutant or *AtMC3* overexpressing plants displayed altered responsiveness to ABA compared with WT or to *atmc3*#13.3 plants complemented with a WT copy of *AtMC3* (*atmc3*#13.3

proAtMC3:AtMC3-GFP). Treatment with ABA has been shown to inhibit seed germination and seedling establishment (Planes *et al.*, 2015; Xu *et al.*, 2020). We observed that the inhibition of germination caused by different ABA concentrations was significantly less severe in *atmc3* mutants and seedlings were able to establish better, indicating that the mutant was less sensitive to the hormone (Figs 4a,b, S6a). Furthermore, since ABA can

promote senescence in detached organs (Song *et al.*, 2016), we treated rosette leaves with ABA and quantified the level of induced senescence by measuring chlorophyll levels. ABA treatment caused a less pronounced decrease in chlorophyll a, the main photosynthetic pigment, in *atmc3* mutants compared with WT plants, indicating that the absence of *AtMC3* may affect ABA-induced senescence (Figs 4c, S6b). Finally, since ABA is a

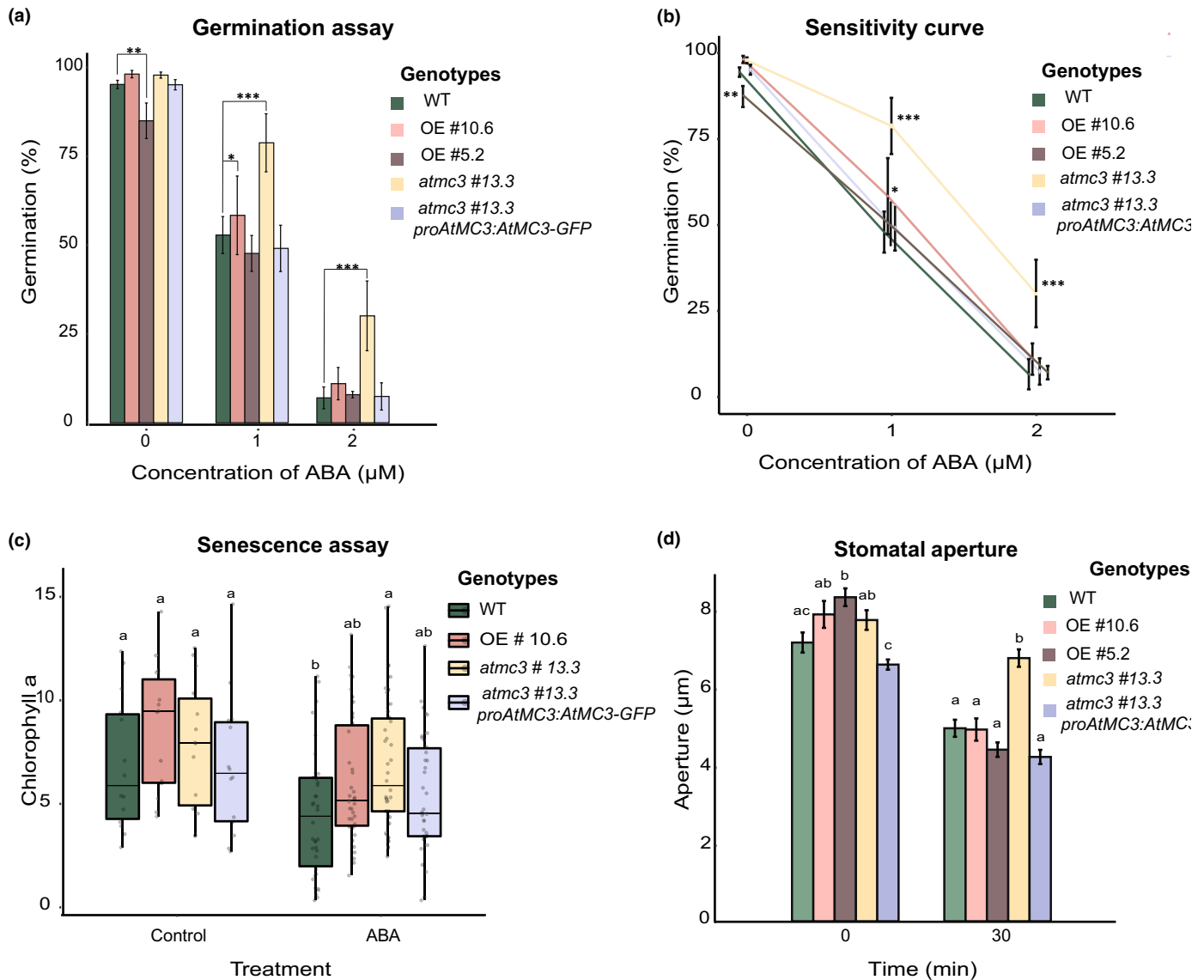


Fig. 4 *AtMC3* null mutants show less sensitivity to abscisic acid (ABA). (a) Germination assay of wild-type (WT), overexpressors, *atmc3*#13.3 mutant, and complemented plants of *AtMC3* with and without ABA treatment. Seeds were germinated on MS-medium plates supplemented with 0 (control), 1 or 2 μM ABA solution and were grown for 8 d before germination rate was calculated. Bar plots are means (\pm SE) from at least three biological replicates per genotype ($n > 90$ per replicate/per genotype). Asterisk indicates significant differences in a chi-squared test for survival ratios compared with WT within every treatment: *, $P < 0.05$; ***, $P < 0.0005$. (b) Dose-response curve for ABA sensitivity of seed germination of WT, overexpressor, *atmc3*#13.3 mutant, and complemented plants of *AtMC3*. ABA concentration ranged from 0 to 2 μM . Error bars represent SE. (c) Senescence assay. Rosette leaves from 5-wk-old plants were cut and incubated with 0 (control) and 50 μM ABA. After 3 d, the amount of chlorophyll a was estimated. Experiments were repeated three times and independent leaves were used to measure the absorbance ($n > 5$ per replicate). Different letters depict significant differences in a one-way ANOVA plus a Tukey's HSD test between the different genotypes and the treatments: $P < 0.005$. (d) Changes in stomatal aperture in WT, overexpressors, *atmc3* #13.3 mutant, and complemented plants after ABA treatment. Cotyledons of 10-d-old plants were treated without (control) or with 10 μM ABA. Bar plots are means from stomatal aperture measurements (\pm SE) from at least three biological replicates per genotype; 30 guard cells were examined in each condition/genotype in all of the three replicates. Different letters depict significant differences in a one-way ANOVA plus a Tukey's HSD test between the genotypes within each treatment: $P < 0.05$.

positive regulator of stomatal closure in response to water deficit, we tested the responsiveness of the plants with altered *AtMC3* levels to ABA treatment by analyzing their ability to close their stomata upon treatment. As shown in Fig. 4(d), stomata of *atmc3* plants were less responsive to ABA after 30 min of treatment compared with all other genotypes tested. Taken together, these results demonstrate that the absence of *AtMC3* results in generalized decreased sensitivity to ABA, which becomes especially evident in the osmotic stress-related responses such as in our stomatal assay.

Overexpression of *AtMC3* confers enhanced drought tolerance

Next, we investigated whether *AtMC3* could play a role in the response to water-deficit conditions that are mainly regulated by ABA (Hossain *et al.*, 2016; Muhammad Aslam *et al.*, 2022). For this, we first compared the survivability of lines with altered *AtMC3* levels to wild-type and *AtMC3* complemented mutant plants to severe drought stress. Water was withheld for 8–9 d in fully grown plants, and the survival rate was calculated after re-watering. Interestingly, plants overexpressing *AtMC3* (independent lines #10.6 and #5.2 tested) showed increased drought tolerance compared with WT plants (Fig. 5a,b). Furthermore, both *atmc3* mutants showed reduced survival rate under drought conditions. The predicted catalytic site did not seem to be required for the drought tolerant role of *AtMC3*, since a transgenic line expressing a version of *AtMC3* with a cysteine to alanine substitution in the putative catalytic site in an *atmc3*#13.3 mutant background (*atmc3* #13.3 *proAtMC3:AtMC3-C230A-GFP*) still restored the survival rate in a WT comparable level under drought conditions (Fig. 5a,b).

Next, we measured water loss through relative water content (RWC), and photosynthetic performance at specific levels of field capacity in plants subjected to drought stress, to ensure that the plants are sensing the same water loss and thus experiencing comparable stress levels. The *AtMC3* overexpressor plants along with the *atmc3* complemented line took 8–9 d to reach 10% field capacity (low water availability), whereas WT and null mutant plants needed only 7 d (Fig. 5c). This suggests that plants overexpressing *AtMC3* can withhold water in a more efficient way and minimize losses while the stress is progressing, a fact that explains

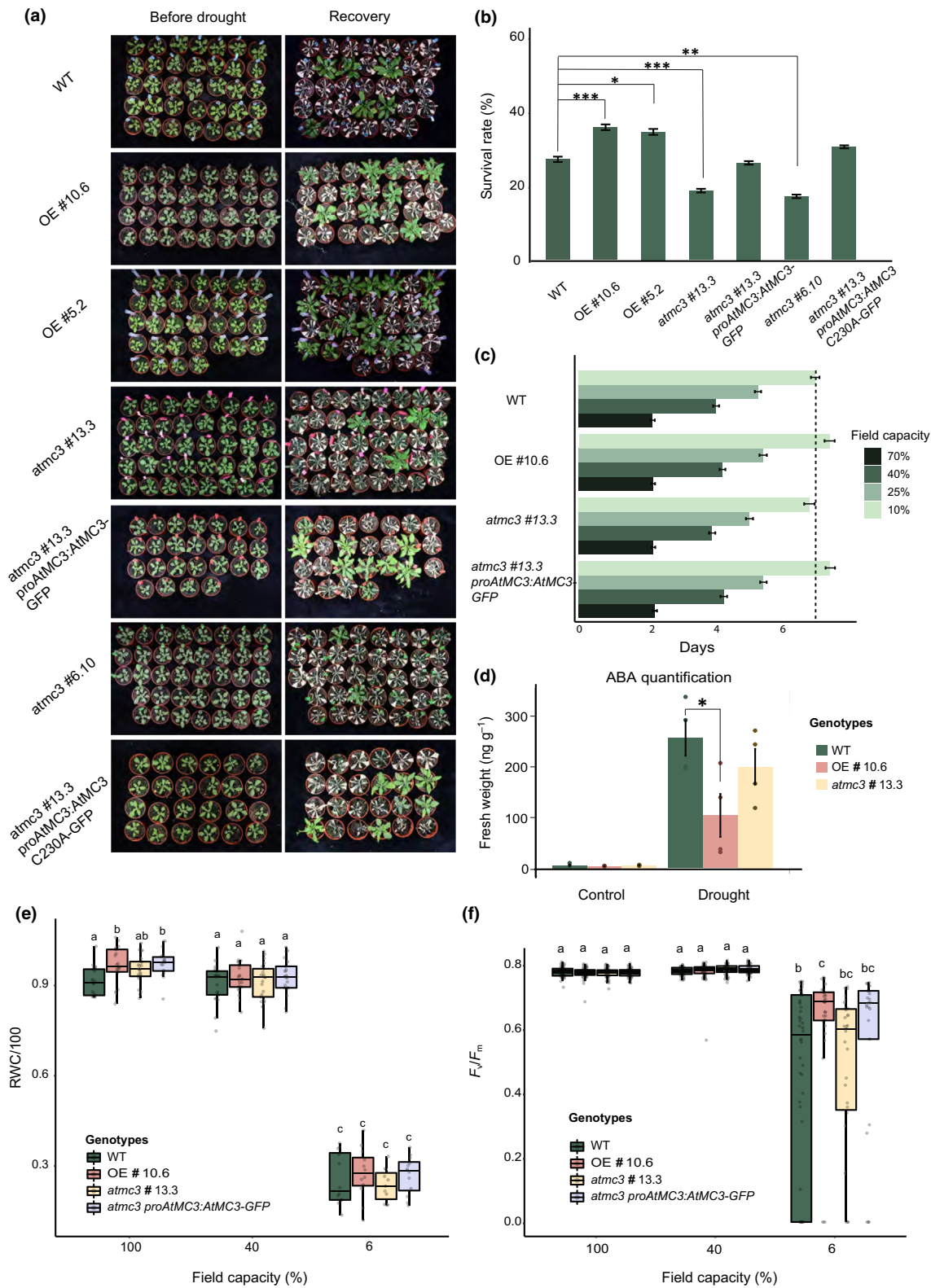
the higher survival detected. In addition, hormonal analysis after 5 d of water deprivation showed that the overexpressor line contained lower levels of ABA and the cytokinin isopentenyl adenosine (IPA), which could be an additional indication of reduced stress-sensed levels (Figs 5d, S7). On the contrary, *atmc3*#13.3 contained elevated levels of salicylic acid (SA) and gibberellin (GA; Fig. S7). GA levels have been shown to be reduced under drought in order to inhibit growth, aiding plants to cope better with the stress (Wang *et al.*, 2008).

Under drought progression (40% and 6% field capacity), there were no differences in RWC observed among the different genotypes. However, in well-watered conditions (100% field capacity), the overexpressor and the *atmc3* complemented line displayed slightly higher water content than the WT plants, which may indicate that they can take better advantage of environmental water when available (Fig. 5e). Maximum quantum yield of photosystem II (F_v/F_m) under severe drought revealed that *AtMC3* overexpressors showed enhanced photosynthesis performance as observed from the less distributed values than WT or *atmc3*#13.3 mutant plants (Figs 5f, S8). In summary, these data may indicate that increasing the levels of *AtMC3* enhances the ability of the plant to cope with drought stress without affecting its growth rates.

The reduced ABA sensitivity displayed by the *atmc3*#13.3 mutant was not attributed to any changes in the expression of ABA biosynthesis genes (*AAO3*), ABA receptors (*PYL5* and *PYL4*), and negative regulators of ABA signaling (*ABI1* and *HABI1*), as demonstrated by gene expression analysis (Fig. 6). However, the transcripts of *RD29A* and *RD22*, two ABA dehydration-responsive genes to maintain the osmotic balance in the cell, were downregulated in *atmc3* when no stress was applied. Moreover, upregulation of *ADH*, a gene that imparts tolerance to multiple stresses including hypoxia and drought (Shi *et al.*, 2017; Rasheed *et al.*, 2018; Ventura *et al.*, 2020), was detected in the *AtMC3* overexpressing lines under normal growth conditions (Figs 6, S4b).

In an attempt to identify potential interactors of the protein, we obtained a large number of proteins that co-immunoprecipitate with *AtMC3* both under mock and drought conditions using plants overexpressing *AtMC3* and WT (Dataset S6, S7). From GO analysis, in drought conditions, 111 out of 600 proteins were related to metabolic processes

Fig. 5 *AtMC3* is involved in drought tolerance. (a) Pictures from 3-wk-old plants before drought stress in well-watered conditions (left column, before drought) and after 5 d of re-watering and recovery (right column, recovery). From top to bottom rosettes of wild-type (WT), OE#10.6, OE#5.2, *atmc3*#13.3, complementation line of the *atmc3*#13.3 mutant, *atmc3*#6.10, and complementation line of *atmc3*#13.3 with a predicted catalytic inactive version of the protein are shown. (b) Plant survival rates calculated as the percentage of plants that survived after 5 d of re-watering relative to the total number of plants used. Bar plots represent averages of 11 independent biological replicates (\pm SE; $n > 150$). Asterisks indicate significant differences in a two-sided chi-squared test for survival ratios compared with WT: *, $P < 0.05$; **, $P < 0.005$; ***, $P < 0.0005$. (c) The number of days (\pm SE) needed to reach different percentages of field capacity for WT, overexpressor, *atmc3*#13.3 mutant, and complementation line are shown in bar plots for five independent replicates ($n > 40$). (d) Abscisic acid (ABA) hormone quantification. Barplots represent the results from four independent replicates in control (well-watered) conditions and 5 d after water withholding when plants started showing wilting symptoms. Student *t*-test was performed to detect significant differences in comparison with the WT in each treatment: *, $P < 0.05$. (e) Relative water content (RWC) of mature rosettes at 100%, 40%, and 6% field capacity. Experiments were repeated four times ($n > 16$). Different letters depict significant differences between genotypes per treatment in a one-way ANOVA plus a Tukey's HSD test: $P < 0.05$. (f) Maximum Quantum Yield of photosynthesis (F_v/F_m) ratio for WT, overexpressor, *atmc3* #13.3 mutant, and complementation line at 100%, 40%, and 6% field capacity. Experiments were repeated four times ($n > 16$). Different letters depict significant differences between genotypes in a one-way ANOVA plus a Tukey's HSD test: $P < 0.05$.



(GO:0006091/GO:0044281), and among those, proteins related to metabolism or transport of osmoprotectants such as sucrose and proline were enriched already in control conditions (Fig. S9a,b; Dataset S8). Furthermore, several of the enriched proteins were related to abiotic stress responses (Fig. S9c), with

some of them reported to show specific vascular expression such as Annexin1 (ANN1) and ABCG11 transporter. ANN1 is responsible for the post-phloem distribution of sugar in the root tip and conferring drought tolerance when overexpressed (Konopka-postupolska *et al.*, 2009; J. Wang *et al.*, 2018).

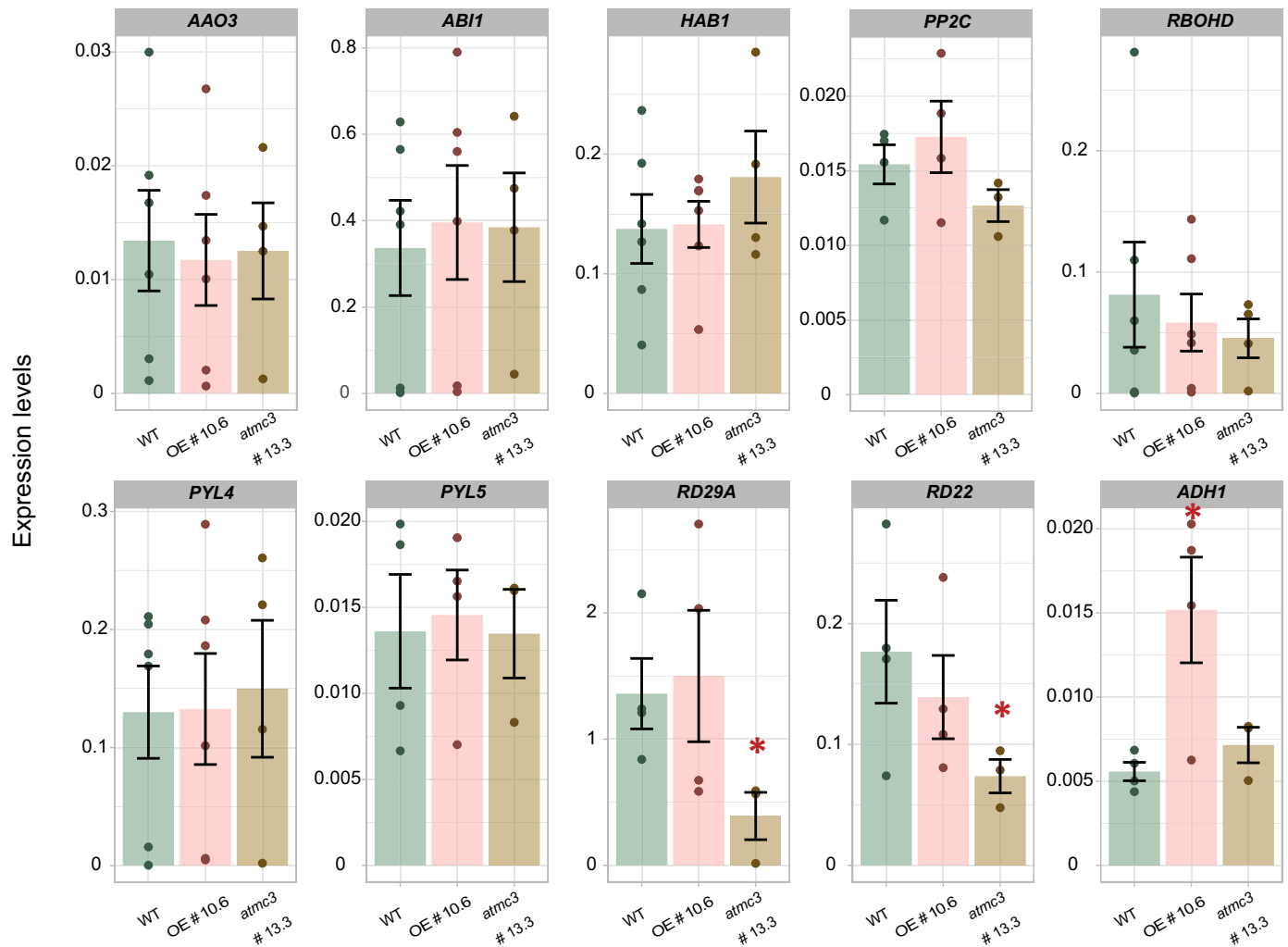


Fig. 6 Expression levels of abscisic acid (ABA)-related genes in plants with altered AtMC3 levels. Expression levels of genes related to ABA biosynthesis (AAO3), downstream signaling (*HAB1*, *ABI1*, *RBOHD*, *PYL4*, *PYL5*, *PP2C*, *RD22*, and *RD29A*), and a target gene (*ADH1*) relative to the housekeeping gene *EIF4a* were analyzed from the cotyledons of 7-d-old seedlings grown in Murashige and Skoog-medium of wild-type (WT), AtMC3 overexpressor, and *atmc3#13.3* mutant plants. Total RNA was extracted and used for cDNA synthesis, which were then used for quantitative PCR analysis. Data correspond to means (\pm SE) from three biological replicates. Significant differences from WT were determined by Student's *t*-test: *, $P < 0.05$.

Aquaporins, dehydrins, and oxidative stress-related proteins were enriched under both control and drought conditions (Fig. S9c). Although limiting, these findings provided hints toward a potential role of AtMC3 in osmotic stress responses.

To determine whether AtMC3 is involved in responses to other osmotic-related stresses, we tested hypoxia and salinity conditions. Under low oxygen conditions (hypoxia), the AtMC3 overexpressing line showed a markedly higher survival rate compared with WT plants, similar to the *prt6* mutant that constitutively induces hypoxia responsiveness through the PCO N-degron pathway (Holdsworth & Gibbs, 2020; Fig. S10a). Interestingly, the *atmc3#13.3* mutant also showed enhanced survival rates under hypoxia conditions. Several hypoxia-marker genes were tested under basal conditions. A clear upregulation of *ADH1* under mock conditions in the AtMC3 overexpressor compared with WT could lead to a better/faster response to hypoxia (Fig. S10b). On the contrary, increased levels of salinity result in inhibition of primary root growth and induce lateral root

formation. Overexpression of AtMC3 resulted in a larger number of lateral roots than WT under salinity stress (Fig. S10c), a phenotype usually observed in plants that display higher salinity tolerance. By contrast, increased levels of salinity resulted in similar levels of primary root growth inhibition in all lines tested (Fig. S10d). In conclusion, our data indicate that AtMC3 may play a role in multiple osmotic stress responses in plants resulting from either excess or absence of water.

Increased AtMC3 levels lead to early metaphloem development and maintain functional transportation under osmotic stress

Considering the specific spatial expression and localization pattern of AtMC3 and its involvement in responses to osmotic stress conditions, we investigated whether stress impinges on the developmental formation of vascular tissues and whether AtMC3 plays a role in these conditions. Upon osmotic stress, root cells lose

water content and accumulate sugars and other osmoprotectant compounds to balance the water shortage from the environment, minimize losses and avoid cellular damage (Sevanto, 2018; Ozturk *et al.*, 2021). As previously documented, incubation of WT plants in media containing sorbitol to cause osmotic imbalance resulted in root growth arrest and a comparable decreased meristematic activity (Cajero-Sanchez *et al.*, 2019), a phenotype also observed in all genotypes tested (Fig. 7a,b).

To better assess whether sorbitol affects phloem development, sorbitol-treated roots were stained with calcofluor white and analyzed by confocal microscopy. Prolonged exposure (72 h) to osmotic stress triggered a premature differentiation of PSEs, as indicated by the appearance of stained cell walls close to the quiescence center (Fig. 7d–h'). While this phenotype was observed in all tested genotypes, > 30% of the roots with altered *AtMC3* levels showed premature differentiation of MSE – either in one or two strands of MSEs – as manifested by their thick cell wall, before the differentiation of protoxylem strands (Fig. 7c,d–h'). In WT plants, this phenotype was also observed in a lesser extent. Metaphloem is the main transport form of the phloem, which functionally replaces the protophloem tissue when the surrounding cell types have already differentiated; thus, its differentiation occurs at *c.* 14 nm above the QC (Rodriguez-Villalon, 2016; Graeff & Hardtke, 2021). Protoxylem differentiation was also measured as the distance from the first spiral cell to the QC in control and stress conditions. We detected that under sorbitol treatment, plants overexpressing *AtMC3* can form protoxylem closer to the QC compared with the rest of genotypes tested, although the meristem size was similar for all of them (Fig. 7i). These data suggest that *AtMC3* levels have an impact on metaphloem and protoxylem differentiation. To elucidate how long-distance transportation is affected in these conditions, we used 5(6)-carboxyfluorescein diacetate (CFDA), a known phloem-mobile probe (Ross-Elliott *et al.*, 2017). CFDA was applied for 1 h on the cotyledons of sorbitol-treated seedlings to ensure its successful loading into the vasculature. Interestingly, we observed that the overexpressing *AtMC3* line #10.6 displayed higher amounts of CFDA in the protophloem unloading zone compared with WT plants in control conditions and under osmotic stress, was able to maintain significantly higher levels of transport compared with the *atmc3* #13.3 plants (Fig. 7j,k). To sum up, fine-tuned levels of *AtMC3* are required for the plants to show the appropriate sensitivity to drought stress by affecting vascular formation; increased levels of the protein to ensure proper function of the tissue.

Discussion

The Arabidopsis type I metacaspase *AtMC3* exhibits a vascular-specific expression pattern concentrated in the phloem pole (Fig. 1; Otero *et al.*, 2022). Our data show that *AtMC3* displays a restricted expression pattern with a shift from the differentiating PSE to the surrounding CCs (Figs 1, S2), similar to multiple genes related to phloem formation such as *APL*, *NAC45/86*, and *CLE45* (Bonke *et al.*, 2003; Rodriguez-Villalon *et al.*, 2014). Furthermore, we demonstrate that the *AtMC3* protein also localizes in the vasculature.

Although altered levels of the protein did not cause any detrimental changes in plant growth and development (Figs 2, S3), proteomic analysis suggested that *AtMC3* is involved in abiotic stress responses. ABA downstream signaling, osmotic, and hypoxia stress-related proteins appeared deregulated in plants with altered *AtMC3* levels, even under control growth conditions (Fig. 3). Multiple peroxidases accumulated to lower levels in plants overexpressing *AtMC3*, potentially indicating changes in the endodermal layer of the root. Additionally, BGLU22, which shows reduced expression upon mannitol treatment (Ahn *et al.*, 2010), accumulated to higher levels in the mutant, while BGLU18 (or ATBG1), involved in the *de novo* biosynthesis of ABA (Lee *et al.*, 2006), showed the opposite behavior. Supporting this data, BGLU18 was found also to co-immunoprecipitate with *AtMC3* under drought stress (Fig. S9c). Interestingly, SASP, a protease that negatively regulates drought responses by leading OST1 to degradation (Q. Wang *et al.*, 2018), was found less abundant in the *AtMC3* overexpressing line. Similarly, we detected reduced accumulation of NAI2, which is involved in ER body formation and was shown to enhance downstream signaling under stress conditions (Kumar *et al.*, 2015). Reduction in NAI2 could be an indication of increased proline accumulation, which assists as an osmoprotectant and improves responses to drought.

ABA has been long considered a 'stress' hormone, as it regulates most of the plant responses to challenging environmental conditions. Plants lacking *AtMC3* showed reduced sensitivity to ABA treatment (Figs 4, S6), which may explain their diminished ability to cope with drought and their increased water losses (Fig. 5b,c). Reduced expression of specific dehydration-responsive genes in *atmc3* mutants could indicate that *AtMC3* may be involved in signaling downstream ABA (Fig. 6). Alternatively, the limited responsiveness to ABA observed in the *atmc3* mutant, particularly under osmotic stress, may suggest that *AtMC3* directly or indirectly participates in long-distance transport of the hormone, mediated by the xylem (Fig. 7i).

We demonstrated that plants overexpressing *AtMC3* were more tolerant to drought stress, as indicated by their increased survival rate and their ability to maintain their photosynthetic capacity more stably (Figs 5, S8). By contrast, *atmc3* mutants survived less compared with WT plants, which was restored by complementing the mutant with both a WT copy of *AtMC3* and a variant version carrying a mutation in the predicted catalytic site. The fact that the predicted protease function of *AtMC3* is not required for its function raises the question of whether the protein might act as a potential stress sensor in CCs. This notion is underscored by the fact that we were not able to detect any direct *AtMC3* proteolytic cleavage from the degradome analyses. In addition, the activity of *AtMC3* or its catalytic mutant could not be assessed biochemically due to the lack of available enzymatic assays for Arabidopsis Type I metacaspases. Interestingly, metacaspases have been proposed to act as homeostatic rheostats, in some cases with functions partly independent of their catalytic activity (Shrestha & Megeny, 2012).

The vascular tissue is a prerequisite for establishing inter-organ communication throughout the plant body. The interaction between phloem and xylem and the maintenance of tissue

plasticity are key for plant adaptation to stress. Sugars are actively loaded into the phloem from source tissues, and the xylem is transferring water into the phloem strands to generate appropriate pressure and flow of the macromolecules. Upon arrival at sink

tissues, sugars are unloaded and distributed while water returns to the xylem files (Sevanto, 2018). Osmotic stress affects the source-sink relationships, and the phloem needs to adjust the osmotic pressure generated from water reduction in the xylem

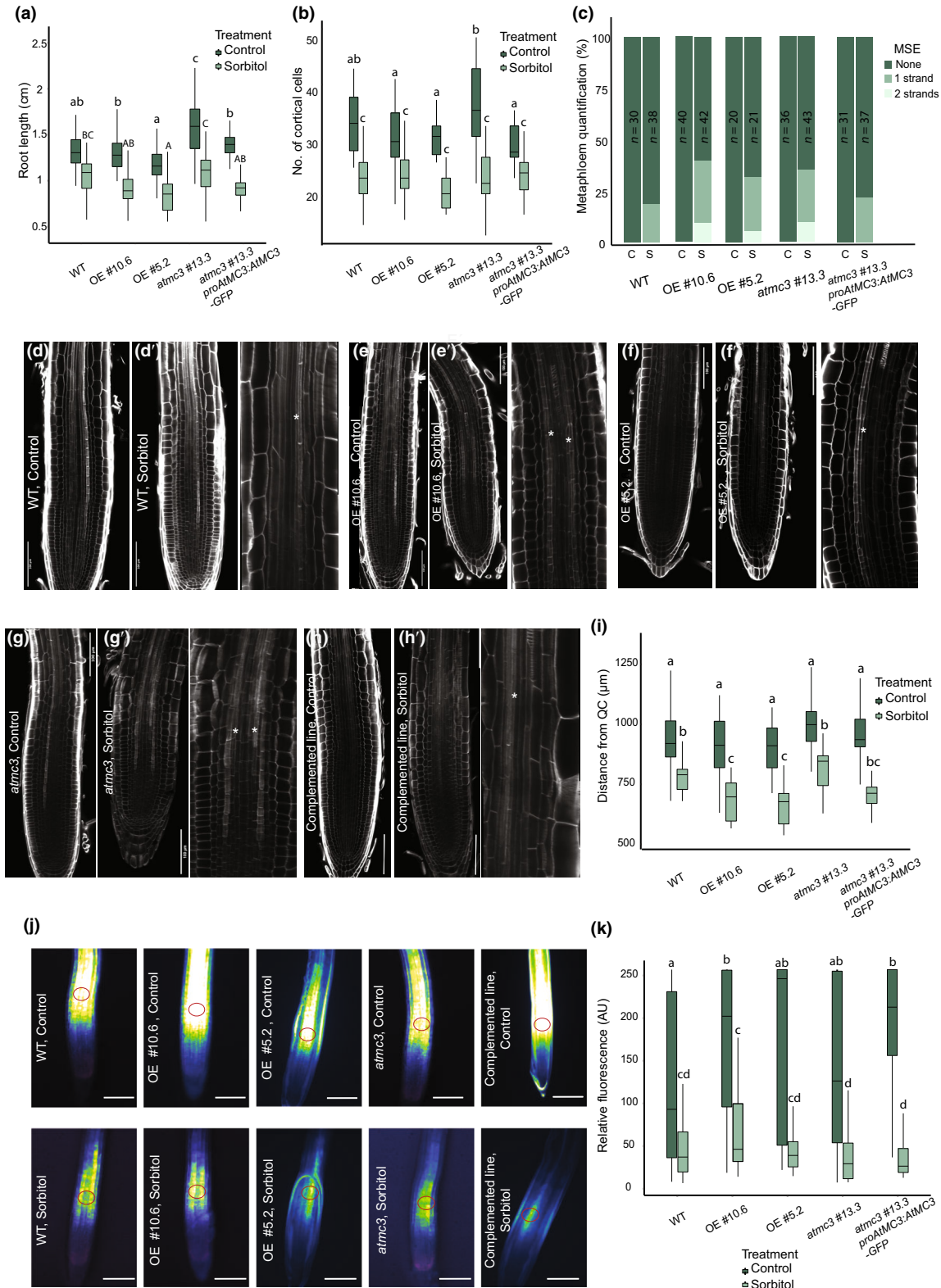


Fig. 7 Vascular tissue formation and function under osmotic stress is affected by AtMC3 levels. (a) Root length and (b) meristem size of 6-d-old seedlings measured from wild-type (WT), overexpressors, *atmc3*#13.3 mutant plants, and complementation line in control (darker green) and under 120 mM sorbitol treatment (lighter green). Box plots represent four biological replicates ($n > 40$ per genotype, per treatment). Different letters depict significant differences in a one-way ANOVA plus a Tukey's HSD test between genotypes under control conditions (small letters) and under sorbitol conditions (capital letters): $P < 0.005$. (c) Percentage of early metaphloem sieve elements (MSE) differentiated earlier than protoxylem strands in none (dark green), one (medium green), or both (light green) MSE strands. C stands for Control and S for sorbitol treatment. (d–h') Indicative pictures from the MSE quantification for the one or both MSE strands affected. Bars, 100 μm . (d', e', f', g', h') for sorbitol treatments. On the right panel is the magnification of the vascular tissue focusing on the phloem strands. Calcofluor staining was used to visualize the roots. White asterisk indicates the differentiated MSE strand. (i) Quantification of protoxylem differentiation distance from the QC for 6-d-old seedlings from WT, overexpressors, *atmc3*#13.3 mutant plants, and complementation line in control (darker green) and under 120 mM sorbitol treatment (lighter green). Experiments were repeated in three independent replicates ($n > 30$ per genotype, per treatment). Different letters depict significant differences in a one-way ANOVA plus a Tukey's HSD test between genotypes and treatments: $P < 0.005$. (j) Representative pictures showing phloem loading from 6-d-old seedlings for WT, overexpressor of AtMC3, and *atmc3* #13.3 mutant in control (upper panels) and sorbitol (lower panels) conditions. Pictures were taken from the root tips c. 1 h after loading CFDA on cotyledons. CFDA fluorescence is visualized in LUT Green Fire Blue. Bar, 500 μm . (k) Quantification of fluorescence intensity in the phloem unloading zone (red circle depicted in j) in WT, overexpressors, *atmc3* #13.3 mutant, and complementation line in 6-d-old seedlings of control and sorbitol-treated plants; bars, 250 μm ; four independent replicates were performed ($n > 30$), and different letters depict significant differences in a one-way ANOVA plus a Tukey's HSD test between genotypes and treatments: $P < 0.05$.

files. An efficient way to achieve this may be by increasing the levels of osmoregulators in the phloem sap (Fàbregas *et al.*, 2018; Sevanto, 2018). Genes involved in vascular development were shown to be affected under osmotic stress (Dinnyen *et al.*, 2008), leading to the speculation that promoting phloem development could increase tolerance. Indeed, we showed that upon osmotic stress, plants form PSE closer to the quiescent center (Fig. 7d–h'). Additionally, altered AtMC3 levels result in premature differentiation of MSE (Fig. 7c). The specific localization of AtMC3 raises the question of whether this protein might be acting as a sensor of stress conditions and what is the role of CCs in signal perception. A functional metaphloem closer to the root tip as observed in the *AtMC3* overexpressing line could provide an advantage to the plants by facilitating the allocation of photoassimilates and osmoprotectant molecules to decrease the water potential in roots or provide the necessary energy for the surrounding tissues to maintain their function and respond. This observation was further supported by the enhanced long-distance transport of CFDA to the root tips in *AtMC3* overexpressor plants (Fig. 7k). Osmotic balance may be maintained more effectively along with the simultaneous induction of xylem differentiation by ABA (Bloch *et al.*, 2019; Ramachandran *et al.*, 2021) as it was observed in the *AtMC3* overexpressing plants (Fig. 7i). Counter-intuitively, the premature metaphloem differentiation observed in the *atmc3* mutant did not result in a similar increase in conductivity, which may suggest that the correct dosage of AtMC3 is required to fine-tune the trade-off between osmotic protection and root development. Although faster protoxylem development was proposed to increased lethality in early seedling stages due to osmotic stress caused by reduced cell wall viscoelasticity (Ramachandran *et al.*, 2021; Augstein & Carlsbecker, 2022), the combination of both vascular tissues might be beneficial for plant survival. Specifically, under drought stress, proteins related to cell wall modification and phloem development (such as CALS8 and SEOB) co-precipitated with AtMC3, highlighting the importance of the cell-border plasticity in plant responses (Dataset S7).

Overall, our results document the role of a vascular metacaspase in osmotic stress responses through a yet-to-be-defined mechanism. The fact that in some instances mutating or overexpressing

AtMC3 led to the same phenotype – slightly longer roots with larger root meristem size and premature MSE differentiation upon osmotic stress – may indicate that the levels of AtMC3 need to be precisely fine-tuned for correct function. Further examining of the potential interactors or substrates of the protein could shed more light about the AtMC3 function under drought stress, which could be addressed with the future development of tissue-specific proteomic approaches. Importantly, AtMC3-overproducing plants are capable of maintaining WT-like growth and yield, unlike other drought-resistant plants reported to date. Severe drought results in significant reduction in dry weight, ultimately resulting in diminished harvested biomass and yield. Therefore, identifying genetic features that may allow for tissue-specific engineering to enhance drought tolerance without compromising plant growth may constitute an extremely valuable strategy for sustainably improving valuable crops.

Statement of limitation of the study

This study has limitations associated with the fact that AtMC3 is a protein exclusively located in the phloem. Considering that our experiments are performed in *Arabidopsis thaliana*, this implies a limitation of tissue to perform certain approaches used in this study such as proteomics or detecting the protein by immunoblot when the transgene was under the control of its native promoter. Therefore, some of the experiments had to be performed using plants constitutively expressing *AtMC3*, with the limitations that this implies in terms of interpretation of the results. Additionally, proteins immunoprecipitating with AtMC3 have not been validated experimentally and therefore are only indicative of potential interactions. Finally, the activity of AtMC3 or its catalytic mutant could not be assessed biochemically due to the reasons described above together with the lack of available enzymatic assays for *Arabidopsis* Type I metacaspases.

Acknowledgements

We kindly thank Marc Planas for starting the work and Fabien Nogu e for sharing CRISPR constructs and expertise. We are

thankful to Moritz Nowack for sharing resources and equipment. We also thank Miguel Ángel Moreno-Risueño and David Blasco-Escámez for inspiring discussions and sharing expertise, Hannah Vahldick for editing the manuscript and Paula Muñoz and Serveis Científico-Tècnics from the University of Barcelona for technical assistance in hormone quantification. Research in the NSC-MV laboratory is funded by project PID2019-108595RB-I00 funded by MCIN/AEI/10.13039/501100011033, TED2021-131457B-I00 funded by MCIN/AEI/10.13039/501100011033, and by the 'European Union NextGenerationEU/PRTR', and through the 'Severo Ochoa Programme for Centres of Excellence in R&D' (SEV-2015-0533 and CEX2019-000902-S funded by MCIN/AEI/10.13039/501100011033). This work was also supported by the CERCA Programme/Generalitat de Catalunya. EP and JS-L were supported by fellowships BES-2016-077242 and BES-2017-080210, respectively, funded by MCIN/AEI/10.13039/501100011033 and by 'ESF Investing in your future'. NR and RdPJ were supported by fellowships FPU2019-03778 and FPU2018-03285, respectively, funded by Ministerio de Universidades. The AR-V laboratory was funded by the Swiss National Foundation, Stavros-Niarchos/ETH-Foundation (EK), and a Swiss government fellowship (RRT). MJH and CD were supported by the University of Nottingham. We acknowledge the support of the publication fee by the CSIC Open Access Publication Support Initiative through its Unit of Information Resources for Research (URICI).

Competing interests

None declared.

Author contributions

EP designed and performed experiments, interpreted data, and wrote the manuscript. RRT designed and performed metaphloem-related experiments and interpreted data. NR-S performed experiments and interpreted data. FD performed LC/MS/MS and analyzed data. EK designed AtMC3 localization experiments and interpreted data. CD performed hypoxia stress experiments and interpreted data. RdPJ and MM performed LC/MS/MS and analyzed data. DV and MS generated AtMC3 promoter-reporter constructs. JS-L performed immunoblots. HH performed GUS stains and interpreted data. HT interpreted data and reviewed the manuscript. FVB provided materials and reviewed the manuscript. MV designed experiments, interpreted data, and reviewed the manuscript. SM-B was in charge of hormone quantification, interpreted data, and reviewed the manuscript. MJH conceptualized hypoxia-related research, interpreted data, and reviewed the manuscript. PFH analyzed LC/MS/MS data and reviewed the manuscript. AR-V conceptualized vascular-related research, designed experiments, interpreted data, and wrote the manuscript. NSC conceptualized the research, designed experiments, interpreted data, and wrote the manuscript.

ORCID

Nuria S. Coll  <https://orcid.org/0000-0002-8889-0399>

Michael J. Holdsworth  <https://orcid.org/0000-0002-3954-9215>
 Pitter F. Huesgen  <https://orcid.org/0000-0002-0335-2242>
 Melissa Mantz  <https://orcid.org/0000-0001-7254-5331>
 Sergi Munné-Bosch  <https://orcid.org/0000-0001-6523-6848>
 Roger de Pedro-Jové  <https://orcid.org/0000-0002-7083-7960>
 Eugenia Pitsili  <https://orcid.org/0000-0001-9180-4650>
 Antia Rodriguez-Villalon  <https://orcid.org/0000-0001-8962-1353>
 Jose Salguero-Linares  <https://orcid.org/0000-0003-0559-7793>
 Hannele Tuominen  <https://orcid.org/0000-0002-4949-3702>
 Marc Valls  <https://orcid.org/0000-0003-2312-0091>
 Frank Van Breusegem  <https://orcid.org/0000-0002-3147-0860>

Data availability

The mass spectrometry proteomics data have been deposited to the ProteomeXchange Consortium (Deutsch *et al.*, 2020) via the PRIDE partner repository (Perez-Riverol *et al.*, 2022). Quantitative proteome data can be accessed with the dataset identifier PXD035957, IP-MS data with the dataset identifier PXD035975.

References

- Ahn YO, Shimizu BI, Sakata K, Gantulga D, Zhou Z, Bevan DR, Esen A. 2010. Scopolin-hydrolyzing β -glucosidases in roots of Arabidopsis. *Plant and Cell Physiology* 51: 132–143.
- Augstein F, Carlsbecker A. 2022. Salinity induces discontinuous protoxylem via a DELLA-dependent mechanism promoting salt tolerance in Arabidopsis seedlings. *New Phytologist* 236: 195–209.
- Band LR, Wells DM, Fozard JA, Ghetiu T, French AP, Pound MP, Wilson MH, Yu L, Li W, Hijazi HI *et al.* 2014. Systems analysis of auxin transport in the Arabidopsis root apex. *Plant Cell* 26: 862–875.
- Bloch D, Puli MR, Mosquana A, Yalovsky S. 2019. Abiotic stress modulates root patterning via ABA-regulated microRNA expression in the endodermis initials. *Development* 146: dev177097.
- Bollhöner B, Zhang B, Stael S, Denancé N, Overmyer K, Goffner D, Van Breusegem F, Tuominen H. 2013. Post mortem function of AtMC9 in xylem vessel elements. *New Phytologist* 200: 498–510.
- Bonke M, Thitamadee S, Mähönen AP, Hauser MT, Helariutta Y. 2003. APL regulates vascular tissue identity in Arabidopsis. *Nature* 426: 181–186.
- Cajero-Sanchez W, Aceves-García P, Fernández-Marcos M, Gutiérrez C, Rosas U, García-Ponce B, Álvarez-Buylla ER, de la Paz Sánchez M, Garay-Arroyo A. 2019. Natural root cellular variation in responses to osmotic stress in *Arabidopsis thaliana* accessions. *Genes* 10: 1–23.
- Chang HY, Yang X. 2000. Proteases for cell suicide: functions and regulation of caspases. *Microbiology and Molecular Biology Reviews* 64: 821–846.
- Coll NS, Vercammen D, Smidler A, Clover C, Van Breusegem F, Dangl JL, Eppe P. 2010. Arabidopsis type I metacaspases control cell death. *Science* 330: 1393–1397.
- Deutsch EW, Bandeira N, Sharma V, Perez-Riverol Y, Carver J, Kundu DJ, García-Seisdedos D, Jarnuczak AF, Hewapathirana S, Pullman BS *et al.* 2020. The ProteomeXchange consortium in 2020: enabling 'big data' approaches in proteomics. *Nucleic Acids Research* 48: 1145–1152.
- Dinneny JR, Long TA, Wang JY, Jung JW, Mace D, Pointer S, Barron C, Brady SM, Schiefelbein J, Benfey PN. 2008. Cell identity mediates the response of Arabidopsis roots to abiotic stress. *Science* 320: 942–945.
- Fàbregas N, Lozano-Elena F, Blasco-Escámez D, Tohge T, Martínez-Andújar C, Albacete A, Osorio S, Bustamante M, Riechmann JL, Nomura T *et al.*

2018. Overexpression of the vascular brassinosteroid receptor BRL3 confers drought resistance without penalizing plant growth. *Nature Communications* 9: 1–13.
- Fausser F, Schiml S, Puchta H. 2014. Both CRISPR/Cas-based nucleases and nickases can be used efficiently for genome engineering in *Arabidopsis thaliana*. *The Plant Journal* 79: 348–359.
- Graeff M, Hardtke CS. 2021. Metaphloem development in the Arabidopsis root tip. *Development* 148: dev199766.
- Gujas B, Kastanaki E, Sturchler A, Cruz TMD, Ruiz-Sola MA, Dreos R, Eicke S, Truernit E, Rodriguez-Villalon A. 2020. A reservoir of pluripotent phloem cells safeguards the linear developmental trajectory of protophloem sieve elements. *Current Biology* 30: 755–766.
- Gupta A, Rico-Medina A, Caño-Delgado AI. 2020. The physiology of plant responses to drought. *Science* 368: 266–269.
- Haeussler M, Schönig K, Eckert H, Eschstruth A, Mianné J, Renaud JB, Schneider-Maunoury S, Shkumatava A, Teboul L, Kent J *et al.* 2016. Evaluation of off-target and on-target scoring algorithms and integration into the guide RNA selection tool CRISPOR. *Genome Biology* 17: 1–12.
- Hander T, Fernández-Fernández ÁD, Kumpf RP, Willems P, Schatowitz H, Rombaut D, Staes A, Nolf J, Pottier R, Yao P *et al.* 2019. Damage on plants activates Ca²⁺-dependent metacaspases for release of immunomodulatory peptides. *Science* 363: eaar7486.
- Hartman S, Liu Z, Van Veen H, Vicente J, Reinen E, Martopawiro S, Zhang H, van Dongen N, Bosman F, Bassel GW *et al.* 2019. Ethylene-mediated nitric oxide depletion pre-adapts plants to hypoxia stress. *Nature Communications* 10: 4020.
- Hartung W, Sauter A, Hoes E. 2002. Abscisic acid in the xylem: where does it come from, where does it go to? *Journal of Experimental Botany* 53: 27–32.
- He R, Drury GE, Rotari VI, Gordon A, Willer M, Farzaneh T, Woltering EJ, Gallois P. 2008. Metacaspase-8 modulates programmed cell death induced by ultraviolet light and H₂O₂ in Arabidopsis. *Journal of Biological Chemistry* 283: 774–783.
- Holdsworth MJ, Gibbs DJ. 2020. Comparative biology of oxygen sensing in plants and animals. *Current Biology* 30: R362–R369.
- Hossain MA, Wani SH, Bhattacharjee S, Burritt DJ, Tran LSP. 2016. *Drought stress tolerance in plants, vol. 2: Molecular and genetic perspectives*. Cham, Switzerland: Springer Cham.
- Konopka-postupska D, Clark G, Goch G, Debski J, Floras K, Cantero A, Fijolek B, Roux S, Hennig J. 2009. The role of annexin 1 in drought stress in Arabidopsis. *Plant Physiology* 150: 1394–1410.
- Kumar MN, Hsieh YF, Verslues PE. 2015. At14a-Like1 participates in membrane-associated mechanisms promoting growth during drought in Arabidopsis thaliana. *Proceedings of the National Academy of Sciences, USA* 112: 10545–10550.
- Kuromori T, Fujita M, Takahashi F, Yamaguchi-Shinozaki K, Shinozaki K. 2022. Inter-tissue and inter-organ signaling in drought stress response and phenotyping of drought tolerance. *The Plant Journal* 109: 342–358.
- Kuromori T, Seo M, Shinozaki K. 2018. ABA transport and plant water stress responses. *Trends in Plant Science* 23: 513–522.
- Kwon SI, Hwang DJ. 2013. Expression analysis of the metacaspase gene family in Arabidopsis. *Journal of Plant Biology* 56: 391–398.
- Lamproulos A, Sutikovic Z, Wenzl C, Maegele I, Lohmann JU, Forner J. 2013. GreenGate – a novel, versatile, and efficient cloning system for plant transgenesis. *PLoS ONE* 8: e83043.
- Lee KH, Piao HL, Kim HY, Choi SM, Jiang F, Hartung W, Hwang I, Kwak JM, Lee I-J, Hwang I. 2006. Activation of glucosidase via stress-induced polymerization rapidly increases active pools of abscisic acid. *Cell* 126: 1109–1120.
- Lema Asqui S, Vercammen D, Serrano I, Valls M, Rivas S, Van Breusegem F, Conlon FL, Dangel JL, Coll NS. 2018. AtSERPIN1 is an inhibitor of the metacaspase AtMCI-mediated cell death and autocatalytic processing in planta. *New Phytologist* 218: 1156–1166.
- Lichtenthaler HK. 1987. Chlorophylls and carotenoids: pigments of photosynthetic biomembranes. *Methods in Enzymology* 148: 350–382.
- Livak KJ, Schmittgen TD. 2001. Analysis of relative gene expression data using real-time quantitative PCR and the 2^{-ΔΔCT} method. *Methods* 25: 402–408.
- McLuskey K, Mottram JC. 2015. Comparative structural analysis of the caspase family with other clan CD cysteine peptidases. *Biochemical Journal* 466: 219–232.
- Minina EA, Coll NS, Tuominen H, Bozhkov PV. 2017. Metacaspases vs caspases in development and cell fate regulation. *Cell Death and Differentiation* 24: 1314–1325.
- Morineau C, Bellec Y, Tellier F, Gissot L, Kelemen Z, Nogué F, Faure JD. 2017. Selective gene dosage by CRISPR-Cas9 genome editing in hexaploid *Camelina sativa*. *Plant Biotechnology Journal* 15: 729–739.
- Muhammad Aslam M, Waseem M, Jakada BH, Okal EJ, Lei Z, Saqib HSA, Yuan W, Xu W, Zhang Q. 2022. Mechanisms of abscisic acid-mediated drought stress responses in plants. *International Journal of Molecular Sciences* 23: 1084.
- Müller M, Munné-Bosch S. 2011. Rapid and sensitive hormonal profiling of complex plant samples by liquid chromatography coupled to electrospray ionization tandem mass spectrometry. *Plant Methods* 7: 37.
- Munns R. 2002. Comparative physiology of salt and water stress. *Plant, Cell & Environment* 25: 239–250.
- Murray MG, Thompson WF. 1980. Rapid isolation of high molecular weight plant DNA. *Nucleic Acids Research* 8: 4321–4326.
- Ogden AJ, Bhatt JJ, Brewer HM, Kintigh J, Kariuki SM, Rudrabhatla S, Adkins JN, Curtis WR. 2020. Phloem exudate protein profiles during drought and recovery reveal abiotic stress responses in tomato vasculature. *International Journal of Molecular Sciences* 21: 4461.
- Ondzighi-Assoume CA, Chakraborty S, Harris JM. 2016. Environmental nitrate stimulates abscisic acid accumulation in Arabidopsis root tips by releasing it from inactive stores. *Plant Cell* 28: 729–745.
- Otero S, Gildea I, Roszak P, Lu Y, Di Vittori V, Bourdon M, Kalmbach L, Bloß B, Heo J-O, Peruzzo F *et al.* 2022. A root phloem pole cell atlas reveals common transcriptional states in protophloem-adjacent cells. *Nature Plants* 8: 954–970.
- Ozturk M, Turkyilmaz Unal B, García-Caparrós P, Khursheed A, Gul A, Hasanuzzaman M. 2021. Osmoregulation and its actions during the drought stress in plants. *Physiologia Plantarum* 172: 1321–1335.
- Perez-Riverol Y, Bai J, Bandla C, Garcia D, Hewapathirana S, Kamatchinathan S, Kundu DJ, Prakash A, Frericks-Zipper A, Eisenacher M *et al.* 2022. The PRIDE database resources in 2022: a hub for mass spectrometry-based proteomics evidences. *Nucleic Acids Research* 50: 543–552.
- Planes MD, Niñoles R, Rubio L, Bissoli G, Bueso E, García-MJ, Alejandro S, Gonzalez-Guzmán M, Hedrich R, Rodriguez PL *et al.* 2015. A mechanism of growth inhibition by abscisic acid in germinating seeds of *Arabidopsis thaliana* based on inhibition of plasma membrane H⁺-ATPase and decreased cytosolic pH, K⁺, and anions. *Journal of Experimental Botany* 66: 813–825.
- Ramachandran P, Augstein F, Mazumdar S, Van Nguyen T, Minina EA, Melnyk CW, Carlsbecker A. 2021. Abscisic acid signaling activates distinct VND transcription factors to promote xylem differentiation in Arabidopsis. *Current Biology* 31: 3153–3161.
- Ramachandran P, Wang G, Augstein F, De Vries J, Carlsbecker A. 2018. Continuous root xylem formation and vascular acclimation to water deficit involves endodermal ABA signalling via miR165. *Development* 145: 1–7.
- Rasheed S, Bashir K, Kim JM, Ando M, Tanaka M, Seki M. 2018. The modulation of acetic acid pathway genes in Arabidopsis improves survival under drought stress. *Scientific Reports* 8: 1–15.
- Rodriguez-Villalon A. 2016. Wiring a plant: Genetic networks for phloem formation in *Arabidopsis thaliana* roots. *New Phytologist* 210: 45–50.
- Rodriguez-Villalon A, Gujas B, Kang YH, Breda AS, Cattaneo P, Depuydt S, Hardtke CS. 2014. Molecular genetic framework for protophloem formation. *Proceedings of the National Academy of Sciences, USA* 111: 11551–11556.
- Ross-Elliott TJ, Jensen KH, Haaning KS, Wager BM, Knoblauch J, Howell AH, Mullendore DL, Monteith AG, Paultre D, Yan D *et al.* 2017. Phloem unloading in Arabidopsis roots is convective and regulated by the phloem pole pericycle. *eLife* 6: 1–31.
- Ruiz Sola MA, Coiro M, Crivelli S, Zeeman SC, Schmidt Kjolner Hansen S, Truernit E. 2017. OCTOPUS-LIKE 2, a novel player in Arabidopsis root and vascular development, reveals a key role for OCTOPUS family genes in root metaphloem sieve tube differentiation. *New Phytologist* 216: 1191–1204.

- Salguero-Linares J, Serrano I, Ruiz-Solani N, Salas-Gómez M, Phukan UJ, González VM, Bernardo-Faura M, Valls M, Rengel D, Coll NS. 2022. Robust transcriptional indicators of immune cell death revealed by spatiotemporal transcriptome analyses. *Molecular Plant* 15: 1059–1075.
- Seo M, Kim H, Lee JY. 2020. Information on the move: vascular tissue development in space and time during postembryonic root growth. *Current Opinion in Plant Biology* 57: 110–117.
- Sevanto S. 2018. Drought impacts on phloem transport. *Current Opinion in Plant Biology* 43: 76–81.
- Shi H, Liu W, Yao Y, Wei Y, Chan Z. 2017. Alcohol dehydrogenase 1 (ADH1) confers both abiotic and biotic stress resistance in *Arabidopsis*. *Plant Science* 262: 24–31.
- Shrestha A, Megeny LA. 2012. The non-death role of metacaspase proteases. *Frontiers in Oncology* 2: 78.
- Song Y, Xiang F, Zhang G, Miao Y, Miao C. 2016. Abscisic acid as an internal integrator of multiple physiological processes modulates leaf senescence onset in *Arabidopsis thaliana*. *Frontiers in Plant Science* 7: 1–16.
- Takahashi F, Kuromori T, Urano K, Yamaguchi-Shinozaki K, Shinozaki K. 2020. Drought stress responses and resistance in plants: from cellular responses to long-distance intercellular communication. *Frontiers in Plant Science* 11: 1–14.
- Tan X, Zwiazek JJ. 2019. Stable expression of aquaporins and hypoxia-responsive genes in adventitious roots are linked to maintaining hydraulic conductance in tobacco (*Nicotiana tabacum*) exposed to root hypoxia. *PLoS ONE* 14: 1–13.
- Tenorio Berrio R, Nelissen H, Inzé D, Dubois M. 2022. Increasing yield on dry fields: molecular pathways with growing potential. *The Plant Journal* 109: 323–341.
- Thalmann M, Santelia D. 2017. Starch as a determinant of plant fitness under abiotic stress. *New Phytologist* 214: 943–951.
- Truernit E, Bauby H, Belcram K, Barthélémy J, Palauqui JC. 2012. OCTOPUS, a polarly localised membrane-associated protein, regulates phloem differentiation entry in *Arabidopsis thaliana*. *Development* 139: 1306–1315.
- Tsiatsiani L, Van Breusegem F, Gallois P, Zavalov A, Lam E, Bozhkov PV. 2011. Metacaspases. *Cell Death and Differentiation* 18: 1279–1288.
- Tyanova S, Temu T, Cox J. 2016. The MAXQUANT computational platform for mass spectrometry-based shotgun proteomics. *Nature Protocols* 11: 2301–2319.
- Uren AG, O'Rourke K, Aravind L, Pisabarro MT, Seshagiri S, Koonin EV, Dixit VM. 2000. Identification of paracaspases and metacaspases: two ancient families of caspase-like proteins, one of which plays a key role in MALT lymphoma. *Molecular Cell* 6: 961–967.
- Ursache R, Andersen TG, Marhavý P, Geldner N. 2018. A protocol for combining fluorescent proteins with histological stains for diverse cell wall components. *The Plant Journal* 93: 399–412.
- Van Bel M, Silvestri F, Weitz EM, Kreft L, Botzki A, Coppens F, Vandepoele K. 2022. PLAZA 5.0: extending the scope and power of comparative and functional genomics in plants. *Nucleic Acids Research* 50(D1): D1468–D1474.
- Ventura I, Brunello L, Iacopino S, Valeri MC, Novi G, Dornbusch T, Perata P, Loreti E. 2020. *Arabidopsis* phenotyping reveals the importance of alcohol dehydrogenase and pyruvate decarboxylase for aerobic plant growth. *Scientific Reports* 10: 1–14.
- Vercammen D, Van De Cotte B, De Jaeger G, Eeckhout D, Casteels P, Vandepoele K, Vandenberghe I, Van Beeumen J, Inzé D, Van Breusegem F. 2004. Type II metacaspases Atmc4 and Atmc9 of *Arabidopsis thaliana* cleave substrates after arginine and lysine. *Journal of Biological Chemistry* 279: 45329–45336.
- Wang C, Yang A, Yin H, Zhang J. 2008. Influence of water stress on endogenous hormone contents and cell damage of maize seedlings. *Journal of Integrative Plant Biology* 50: 427–434.
- Wang J, Song J, Clark G, Roux SJ, Advanced T. 2018. ANN1 and ANN2 function in post-phloem sugar transport in root tips to affect primary root. *Growth* 178: 390–401.
- Wang Q, Guo Q, Guo Y, Yang J, Wang M, Duan X, Niu J, Liu S, Zhang J, Lu Y *et al.* 2018. *Arabidopsis* subtilase SASP is involved in the regulation of ABA signaling and drought tolerance by interacting with OPEN STOMATA 1. *Journal of Experimental Botany* 69: 4403–4417.
- Watanabe N, Lam E. 2005. Two *Arabidopsis* metacaspases AtMCP1b and AtMCP2b are arginine/lysine-specific cysteine proteases and activate apoptosis-like cell death in yeast. *Journal of Biological Chemistry* 280: 14691–14699.
- Weng SSH, Demir F, Ergin EK, Dirnberger S, Uzoie A, Tuscher D, Nierves L, Tsui J, Huesgen PF, Lange PF. 2019. Sensitive determination of proteolytic proteoforms in limited microscale proteome samples. *Molecular and Cellular Proteomics* 18: 2335–2347.
- Xu D, Wu D, Li XH, Jiang Y, Tian T, Chen Q, Ma L, Wang H, Deng XW, Li G. 2020. Light and abscisic acid coordinately regulate greening. *Plant Physiology* 183: 1281–1294.
- Zahra N, Hafeez MB, Shaikat K, Wahid A, Hussain S, Naseer R, Raza A, Iqbal S, Farooq M. 2021. Hypoxia and anoxia stress: plant responses and tolerance mechanisms. *Journal of Agronomy and Crop Science* 207: 249–284.
- Zhang X, Henriques R, Lin SS, Niu QW, Chua NH. 2006. Agrobacterium-mediated transformation of *Arabidopsis thaliana* using the floral dip method. *Nature Protocols* 1: 641–646.

Supporting Information

Additional Supporting Information may be found online in the Supporting Information section at the end of the article.

Dataset S1 List of 1072 proteins quantified *Arabidopsis thaliana* root samples from Col-WT, *atmc3* #13.3 crisper mutant, and overexpressor line seedlings.

Dataset S2 List of proteins with significant changes in abundance between overexpressor and WT root samples.

Dataset S3 List of proteins with significant changes in abundance between overexpressor and *atmc3* #13.3 crisper mutant root samples.

Dataset S4 GO enrichment for Biological Process ontology in preHUNTER experiments of proteins with significantly altered levels when AtMC3 was compared with WT.

Dataset S5 List of proteins with significant changes in abundance between *atmc3*#13.3 crisper mutant and WT root samples.

Dataset S6 Complete list of proteins that co-immunoprecipitated with AtMC3 in control and drought conditions in comparison with the WT plants under the same respective conditions.

Dataset S7 Complete list of proteins that co-immunoprecipitated with AtMC3 only in drought conditions.

Dataset S8 GO enrichment for Biological Process ontology in drought conditions of proteins co-immunoprecipitated with AtMC3 compared with WT.

Fig. S1 Localization of AtMC3 promoter activity in transgenic lines carrying *proAtMC3-GUS* promoter fusions.

Fig. S2 Localization pattern of AtMC3 catalytic inactive version of protein in roots.

Fig. S3 Phenotypical analysis of AtMC3 overexpressor and mutant lines.

Fig. S4 QPCR analysis.

Fig. S5 Proteomic analysis in root tissue between WT and *atmc3#13.3* mutant plants.

Fig. S6 ABA sensitivity assays.

Fig. S7 Hormonal profile in plants with different AtMC3 levels under drought.

Fig. S8 Efficiency of PSII in severe drought stress.

Fig. S9 AtMC3 interactome analysis.

Fig. S10 AtMC3 is involved in responses to multiple abiotic stresses.

Table S1 Transgenic and mutant lines used in this study.

Table S2 Primers used for cloning strategies and genotyping.

Table S3 Primers used in qPCR analysis.

Please note: Wiley is not responsible for the content or functionality of any Supporting Information supplied by the authors. Any queries (other than missing material) should be directed to the *New Phytologist* Central Office.